

# Coordinates

Volume XVIII, Issue 8, August 2022

THE MONTHLY MAGAZINE ON POSITIONING, NAVIGATION AND BEYOND



## Laser scanning in archaeology and cultural heritage documentation

NRTK observations and their uncertainties in a modern datum



**0.05°**  
ATTITUDE

**0.02°**  
HEADING

**1 cm**  
POSITION

## NEW ELLIPSE-D

### The Smallest Dual Frequency & Dual Antenna INS/GNSS

- » RTK Centimetric Position
- » Quad Constellations
- » Post-processing Software



**Ellipse-D**  
RTK Dual Antenna



**Ellipse-N**  
RTK Single Antenna



**OEM**  
RTK Best-in-class SWaP-C

# RIEGL MOBILE MAPPING SYSTEMS

CHOOSE THE SYSTEM THAT PERFECTLY MEETS YOUR REQUIREMENTS TO SATISFY YOUR CLIENTS' TASKS!

<p>100 scan lines/sec 200 kHz eff. meas. rate</p> <p>up to 4 cameras including spherical camera</p> <p><i>typ. point density 350 points/m<sup>2</sup> on pavement surface @ 80 km/h</i></p>	<p>200 scan lines/sec 400 kHz eff. meas. rate</p> <p>up to 4 cameras including spherical camera</p> <p><i>typ. point density 700 points/m<sup>2</sup> on pavement surface @ 80 km/h</i></p>	<p>250 scan lines/sec 1.8 MHz eff. meas. rate</p> <p>up to 4 cameras including spherical camera</p> <p>multiple swivel positions for improved scan pattern in multi-pass applications</p> <p><i>typ. point density 3,200 points/m<sup>2</sup> on pavement surface @ 80 km/h</i></p>	<p>500 scan lines/sec 3.6 MHz eff. meas. rate</p> <p>up to 9 cameras including spherical camera and up to 2 high-speed pavement cameras</p> <p>simultaneous capturing of spherical and directional imagery with a total resolution of up to 1370 MP/sec</p> <p><i>typ. point density 6,400 points/m<sup>2</sup> on pavement surface @ 80 km/h</i></p>
---	---	---	---

VMY-1

VMY-2

VMQ-1HA

VMX-2HA

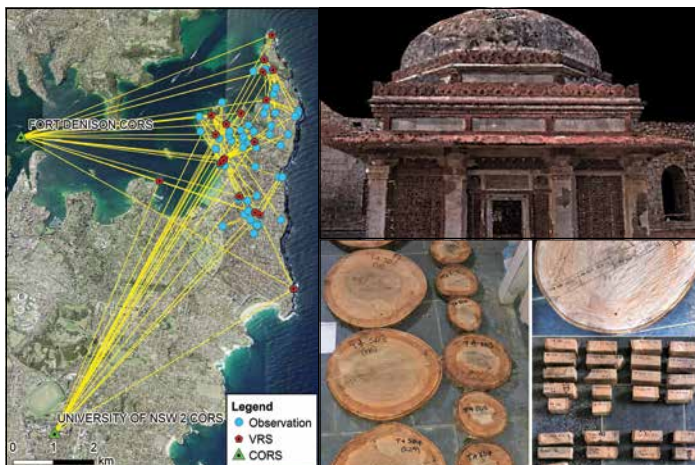
**A broad system portfolio serving all levels of applications:**

transportation infrastructure mapping, city modeling, GIS mapping & asset management, road surface management, open-pit mine surveying, rapid capture of construction sites and bulk material, HD mapping for autonomous vehicles



Explore the full portfolio of proven RIEGL LIDAR Sensors and Systems at [www.riegl.com](http://www.riegl.com)





# In this issue

Coordinates Volume 18, Issue 8, August 2022

## Articles

- Laser scanning in archaeology and cultural heritage documentation** HINA PANDE, POONAM SETH TIWARI AND SHEFALI AGARWAL 7 **NRTK observations and their uncertainties in a modern datum** TOM BERNSTEIN AND VOLKER JANSSEN 12 **New insights into large tropical tree mass and structure from direct harvest and terrestrial lidar** ANDREW BURT, MATHEUS BONI VICARI, ANTONIO C L DA COSTA, INGRID COUGHLIN, PATRICK MEIR, LUCY ROWLAND AND MATHIAS DISNEY 17

## Columns

- My Coordinates** EDITORIAL 5 **Old Coordinates** 31 **News** GIS 32 GNSS 33 IMAGING 34 LBS 35 INDUSTRY 35 **Mark Your Calendar** 38

This issue has been made possible by the support and good wishes of the following individuals and companies

Andrew Burt, Antonio C L da Costa, Hina Pande, Ingrid Coughlin, Lucy Rowland, Matheus Boni Vicari, Mathias Disney, Patrick Meir, Poonam Seth Tiwari, Shefali Agarwal, Tom Bernstein and Volker Janssen; GPSatsy, Labsat, Riegl, SBG System, and many others.

### Mailing Address

A 002, Mansara Apartments  
C 9, Vasundhara Enclave  
Delhi 110 096, India.

**Phones** +91 11 42153861, 98102 33422, 98107 24567

### Email

[information] talktous@mycoordinates.org

[editorial] bal@mycoordinates.org

[advertising] sam@mycoordinates.org

[subscriptions] iwant@mycoordinates.org

**Web** www.mycoordinates.org

Coordinates is an initiative of CMPL that aims to broaden the scope of positioning, navigation and related technologies.

CMPL does not necessarily subscribe to the views expressed by the authors in this magazine and may not be held liable for any losses caused directly or indirectly due to the information provided herein. © CMPL, 2022. Reprinting with permission is encouraged; contact the editor for details.

**Annual subscription** (12 issues)

[India] Rs.1,800 [Overseas] US\$100

**Printed and published** by Sanjay Malaviya on behalf of Coordinates Media Pvt Ltd

**Published** at A 002 Mansara Apartments, Vasundhara Enclave, Delhi 110096, India.

**Printed** at Thomson Press (India) Ltd, Mathura Road, Faridabad, India

**Editor** Bal Krishna

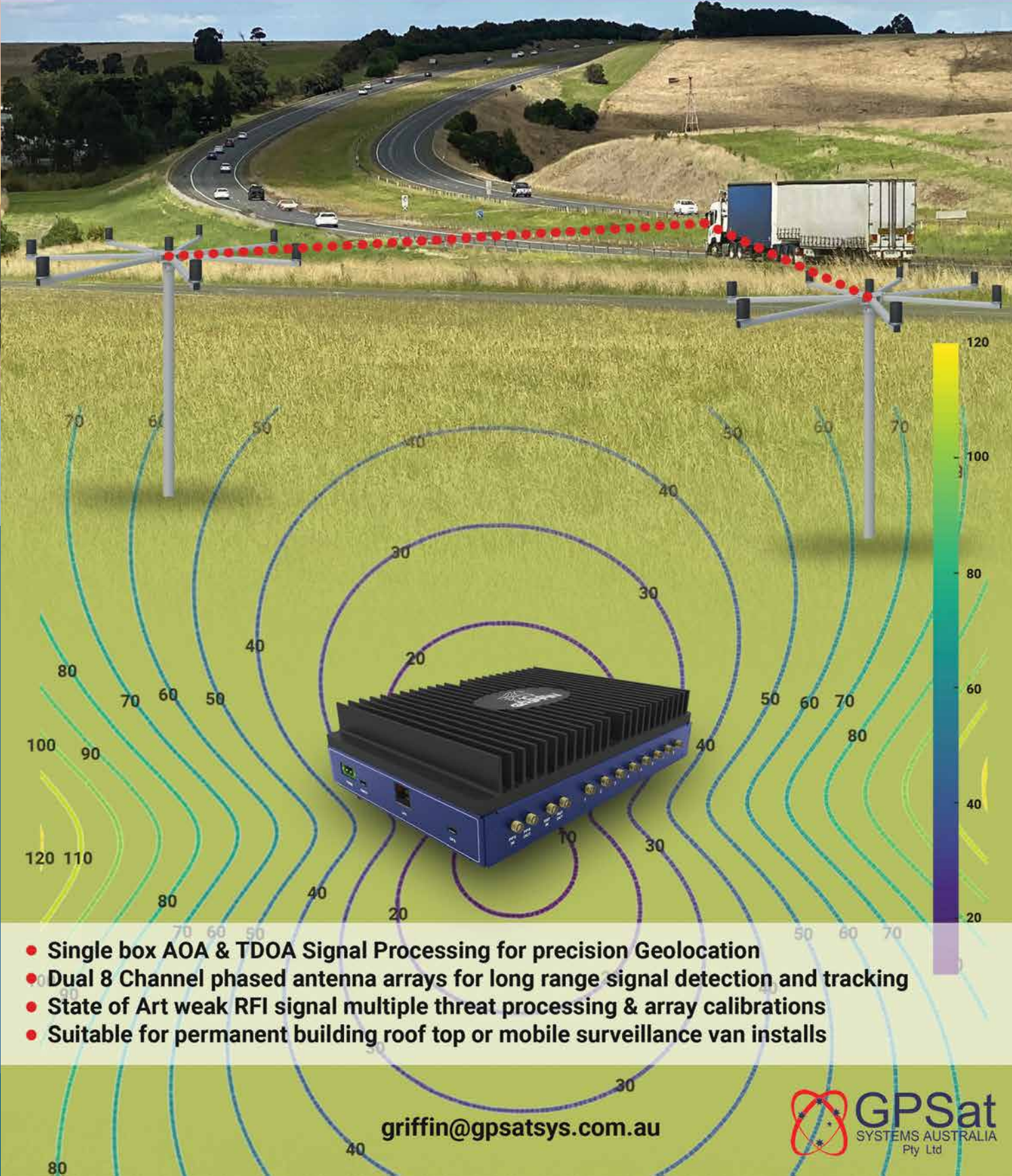
**Owner** Coordinates Media Pvt Ltd (CMPL)

This issue of Coordinates is of 40 pages, including cover.



# EMBASSY

PRECISION GEOLOCATION OF MULTIPLE GNSS  
JAMMING & SPOOFING THREATS GNSS SPECTRUM PROTECTION



- Single box AOA & TDOA Signal Processing for precision Geolocation
- Dual 8 Channel phased antenna arrays for long range signal detection and tracking
- State of Art weak RFI signal multiple threat processing & array calibrations
- Suitable for permanent building roof top or mobile surveillance van installs

[griffin@gpsatsys.com.au](mailto:griffin@gpsatsys.com.au)





Recently, an Immarsat led team of companies in the UK

Began the broadcasting satellite navigation signal.

This was done in coordination with the U.S. Federal Aviation Administration (FAA), the European Space Agency (ESA) and the European Union Space Programme Agency (EUSPA).

And was intended to explore the national capability in resilient PNT.

The UK Space-Based Augmentation System (UKSBAS) generates an overlay test signal to the U.S. GPS to increase the accuracy of positioning.

This is a significant development as the UK is no longer the part of Galileo system,

And cannot use European Geostationary Navigation Overlay Service (EGNOS) safety of life (SOL) services.

The tests will assess whether UKSBAS can develop into a full operational capability to support safety-critical applications in aviation and maritime sector.

And may be a step forward towards full-fledged UK GNSS?

Bal Krishna, Editor  
bal@mycoordinates.org

**ADVISORS** Naser El-Sheimy PEng, CRC Professor, Department of Geomatics Engineering, The University of Calgary Canada, George Cho Professor in GIS and the Law, University of Canberra, Australia, Professor Abbas Rajabifard Director, Centre for SDI and Land Administration, University of Melbourne, Australia, Luiz Paulo Souto Fortes PhD Associate Professor, University of State of Rio Janeiro (UERJ), Brazil, John Hannah Professor, School of Surveying, University of Otago, New Zealand

# Laser scanning in archaeology and cultural heritage documentation

The remote sensors play a significant role in field archaeology as they offer non-invasive means for collecting data related to the physical and chemical properties of objects from space based, aerial and terrestrial platforms.



**Hina Pande**  
Indian Institute of Remote Sensing (ISRO)  
Dehradun, India



**Poonam Seth Tiwari**  
Indian Institute of Remote Sensing (ISRO)  
Dehradun, India



**Shefali Agarwal**  
Indian Institute of Remote Sensing (ISRO)  
Dehradun, India

Indian heritage and culture are vast and vivid, encompassing both tangible and intangible elements. With numerous archaeological sites spread across the whole country, a tool like remote sensing and geographic information system has high potential for exploring these, especially the built heritage. These tools and methods help in establishing certain facts about the sites that may not be possible to achieve from other conventional methods. The remote sensors play a significant role in field archaeology as they offer non-invasive means for collecting data related to the physical and chemical properties of objects from space based, aerial and terrestrial platforms. (Parack,2017)

The archaeologists and historians, involved in various activities connected to heritage preservation and research would find the technology greatly beneficial since digital tools such as 3D scanning are providing increasingly detailed and accurate information within a relatively shorter time span.(Bassier,2018)

Lidar, which stands for Light Detection and Ranging, is a remote sensing method for determining ranges by targeting an object or a surface with a laser and measuring the time for the reflected light to return to the receiver. Each laser pulse can produce multiple consecutive measurements from reflections off several surfaces in its path. It can also be used to make digital 3-D representations of

areas on the earth’s surface and ocean bottom by varying the wavelength of light, in other words the technique can generate accurate 3D information about the earth surface and the target object.

LiDAR systems are most commonly used for surveying tasks i.e. their ability to collect three dimensional measurements, surveying the built environment (such as buildings, road networks and railways), creating digital terrain (DTM) and elevation models (DEMs) of specific landscapes. However the technique can be used for a myriad of applications in civil engineering, corridor applications(power utility, railway etc), archaeology, forestry, mining, environmental research and disaster management work; to name a few.

The laser scanners are preferred mode for 3D data acquisition due to advantages like high data density, fast data acquisition with minimum human dependence, high range of accuracy, independent of illumination and weather conditions to a great extent, ability to penetrate vegetation canopy unlike photogrammetry. These characteristics make laser scanners especially useful for application in cultural heritage documentation and archaeological studies.

Cultural heritage refers to the physical and cultural assets, both tangible and non-tangible, passed on to us by our previous generations. Historical structures are one of the most significant elements of cultural

heritage. They reflect history, lifestyle and tradition of a country and society. In the current scenario cultural heritage is threatened by various factors such as natural hazards, vandalism, development of cities, and natural aging. Built heritage is an essential aspect of cultural heritage. The built heritage also referred as monuments, have suffered significant damage especially in India, majorly due to human activity and population pressure. Hence, proper mapping, damage detection and digital documentation of cultural heritage sites thus becomes essential for their preservation and protection (Remodino et al., 2007)

Approaches for comprehensive digital documentation of cultural heritage need to be developed; employing techniques and instruments which are capable of providing multi-dimensional information in quick and easy manner. This would enable effective monitoring and conservation of monuments and heritage sites (Prasanna et al., 2012)

New technologies and a growing need to document and preserve information and objects related to cultural heritage is expanding at a rapid rate. 3D documentation, multiscale database of monument and digital blueprinting of heritage structures provides the necessary details and information for constructing heritage inventories, assessing damages/ risk and management and monitoring the built heritage sites. However, despite all these potential applications, a systematic and targeted use of 3D surveying and modelling in the cultural heritage field is still not yet employed in our country. Many studies have proved that terrestrial laser scanner is a powerful tool towards recording of objects and sites for heritage preservation purposes, scientific research and built environment applications. However, widespread practical application by users is lacking hence in order to utilise the technology for practical operational work, a set of standard operating procedure needs to be developed. This will enable easy understanding of the complex technique and instrumentation by non-experts. The objective is to demonstrate

how technically advanced ground based instruments e.g. TLS, GPS etc can help to improve the conventional standards of heritage recording and documentation and utilize geospatial technology for digital documentation of cultural sites.

It is seen that terrestrial laser scanning (TLS) along with close range photogrammetry has immense potential in documentation of heritage monuments. Once a detailed digital model is available, a standard operating procedure for digital documentation and automated damage assessment of built heritage sites can be developed.

Documentation process using TLS primarily aims to create geometric and photorealistic 3D models for both precise reconstruction and visualization (Besl and McKay, 1992). Over the last two decades, the documentation of cultural heritage using terrestrial laser scanning (TLS) technique has significantly increased (Remondino, and Campana, 2014). This fact is mainly due to the wide availability of laser scanning technology and its ability to provide dense surface models in a short period of time with accuracy and reliability.

The capability of capturing dense, ultra-high resolution points with associated x,y,z coordinates and RGB values makes the technique suitable for acquiring the finer details of artefacts/architecture.

A few UNESCO World heritage sites of northern India viz. Humayun's tomb, Qutub Complex (Delhi) and Nalanda Mahavihar (Bihar) have been taken up to demonstrate the potential of 3D data and models for historical site documentation. The utility of using remote sensors to carry out a comprehensive (internal and external) multiscale documentation of heritage monuments, which would enable digital blue printing and damage detection at very high resolutions is explored. The case example of the Qutub Complex (Delhi) is described here since the Monuments of Qutub Complex display an interesting blend of variety and complexity of structure e.g. a vertical tapering tower with considerable height, extensively damaged structures and wide expanse of the site. Figure 1 displays the map location of the Qutub Complex, the complex boundary is also overlaid on satellite image along with field photo and laser scan data of the Minar.

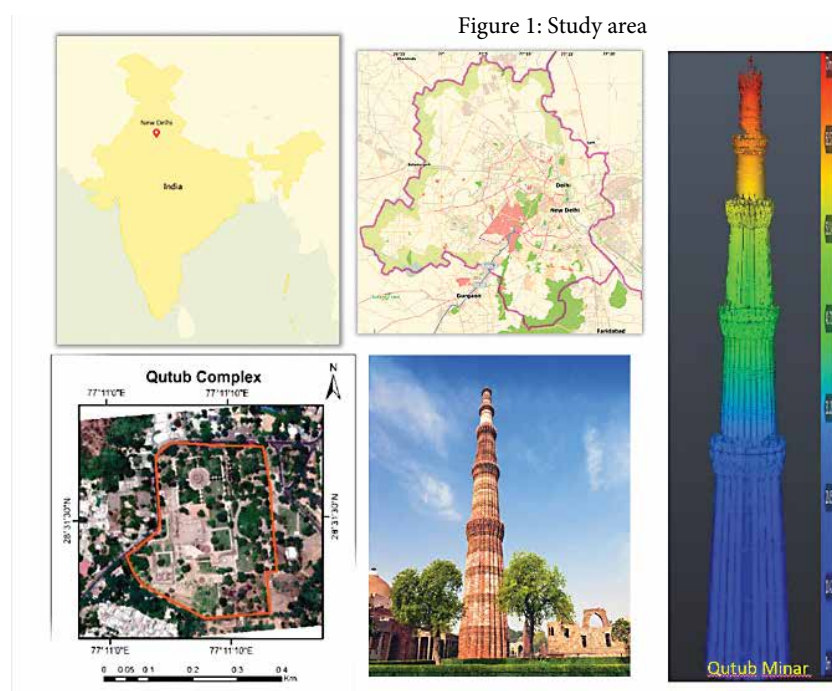


Figure 1: Data Preprocessing and Integration a: Far range point cloud, b: Near range point cloud, c: Integrated Point cloud, d: Point cloud depicting height



## Procedural workflow

### i. Data acquisition, Integration and Generation of 3D model:

Since the monuments have complex shape, vast expanse and height and tapering structures, calculating the amount of overlap and the number of scans required to cover the structure in its entirety becomes complicated and needs careful planning. The shape of the structures is generalized and multiple scans are acquired with a higher overlap percentage of 90% to capture the details of structure and its engravings.

The TLS point cloud was filtered, and individual scans were co-registered to generate 3D point cloud. Point clouds obtained from different scans, covering the entire site were merged and aligned to get the final merged point cloud.

### ii. Extraction of Architectural Elements and Digital Blue Printing:

Architectural elements are the unique details and component parts that, together, form the architectural style of the monuments. To extract the architectural elements the coloured and textured point cloud was smoothed by means of a smoothing filter and was then subjected to edge extraction technique, which resulted in extraction of significant edges. The geometrical inaccuracies in the preliminary boundaries obtained from above approach needs to be corrected and refined before the drawing of individual architectural elements can be created. Image processing based algorithms were applied on the preliminary boundaries. This approach was successful in refining the major edges; however blue printing requires minute detailing also. Hence manual editing was required in certain portions, for proper representation of the architectural elements. Figure 3 shows the entire procedure applied on a section of Tomb of Imam Zamin within the Qutub complex.

The procedure was applied to other sections of the point cloud representing different architectural elements, which were extracted using the automated

method. The individual elements were integrated to result in a digital blue print of the monument (Figure 4).

The digital blueprints so generated are the preliminary step to deal with aspects of heritage documentation and management. These blueprints provide a very diverse range of data (quantitative and qualitative) which can be investigated to produce an accurate digital representation of the building. It can also play a key role in preparing a Heritage Building Information

Modelling (H-BIM) system for effective management of the different aspects of dealing with heritage buildings. Examples of ultra-high resolution 3D models of some structures within the Qutub Heritage Complex are shown in figure 5

Data acquisition and analysis methods utilising non-invasive technology e.g. LiDAR are also ideal for applications such as structural health assessment of monuments. Such data when combined with advanced image processing

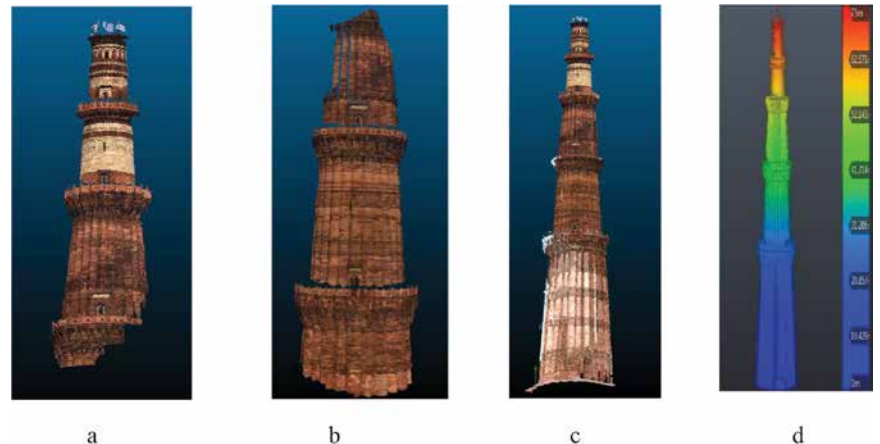


Figure 2: Data Preprocessing and Integration a-b: Individual point clouds from different locations, c: Integrated Point cloud, d: Coloured Point cloud depicting height variation

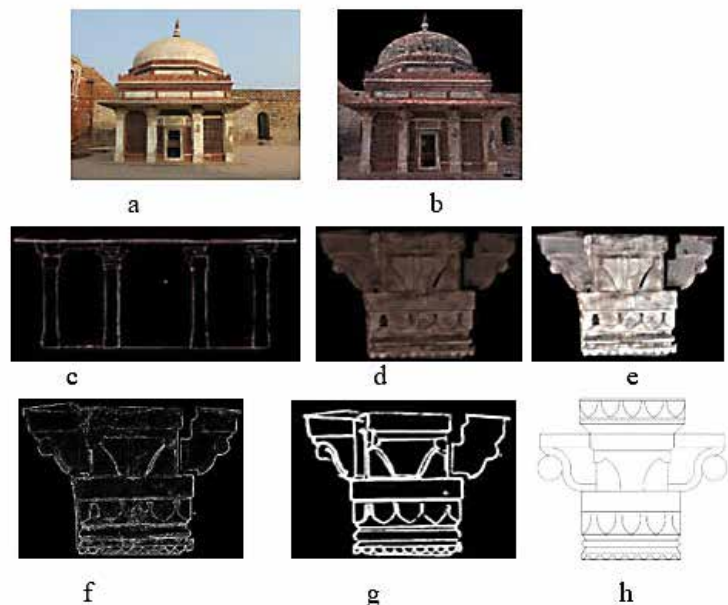


Figure 3: Extraction and refinement of architectural elements. a) Tomb of Imam Zamin; b) Textured point cloud; c) Extracted Pillars d) original point cloud for part of pillar; e) smoothed point cloud; f) Extracted edges; g) Edge refinement with active contours; h) After manual refinement and editing

techniques help in identifying damages, such as cracks, broken parts, discolorations etc, virtual reconstruction of broken patterns or artefacts and conjectural reconstruction. These realistic three dimensional models with associated attributes can also be used as primary data to create digital museums and other interactive virtual environments.

Therefore the 3D models and metric products are useful for creating a detailed multiscale database of monument and a

precise digital blueprint of built heritage structures. It provides a tool for damage detection using point clouds and multiscale representation of structure for monitoring, assessment and reconstruction.

In conclusion, this is not only an example of effective and operational use of latest digital surveying techniques especially terrestrial laser scanners for digital documentation, 3D visualization, damage detection and monitoring of built structures; heritage monuments

in particular but also represents the prospect of enabling preventive measures for maintenance and decision-making and heritage management .

## References

Bassier, M.; An Overview of Innovative Heritage Deliverables Based on Remote Sensing Techniques. *Remote Sens.* 2018, 10(10), 1607; <https://doi.org/10.3390/rs10101607>.


Besl, Paul J. and McKay, Neil D. "Method for registration of 3-D shapes", Proc. SPIE 1611, Sensor Fusion IV: Control Paradigms and Data Structures, (30 April 1992); <https://doi.org/10.1117/12.57955>

Parcak, S.H; GIS, Remote Sensing, and Landscape Archaeology.(2017) DOI: 10.1093/oxfordhb/9780199935413.013.11 (Accessed March 30, 2022).

Prasanna, P. , Dana K., Gucunski, N. , and Basily B.(2012) "Computer-vision based crack detection and analysis", Proc. SPIE 8345, Sensors and Smart Structures Technologies for Civil, Mechanical, and Aerospace Systems 2012, 834542; <https://doi.org/10.1117/12.915384>

Remondino, F. and Campana, S., 2014. 3D recording and modelling in archaeology and cultural heritage. BAR international series, 2598, pp.111-127.

Remondino, F., Rizzi, A. Reality-based 3D documentation of natural and cultural heritage sites—techniques, problems, and examples. *Appl Geomat* 2, 85–100 (2010). <https://doi.org/10.1007/s12518-010-0025-x>

Sevara, C., M. Pregesbauer, M. Doneus, G. Verhoeven, and I. Trinks (2016). Pixel Versus Object—A Comparison of Strategies for the Semi-Automated Mapping of Archaeological Features Using Airborne Laser Scanning Data.” *Journal of Archaeological Science* 5: 485– 498. 

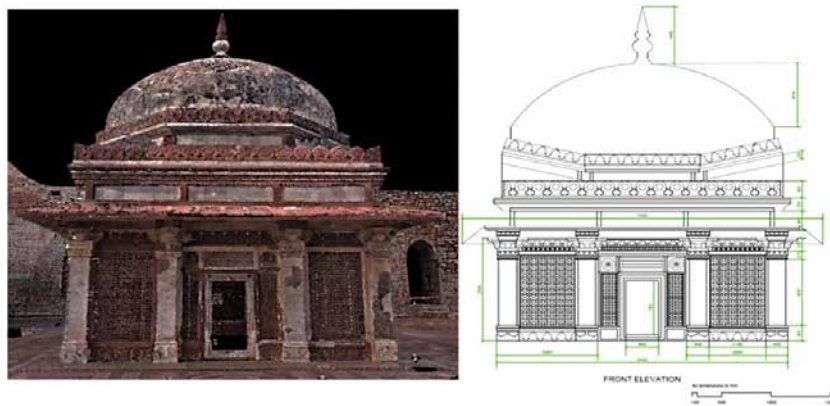


Figure 4: Laser scan derived blue print for Tomb of Imam Zamin, Qutub Complex, New Delhi



Figure 5 a: Ultra-dense laser scan of intricate pillar carvings, statues, tombs: Photorealistic visualisati

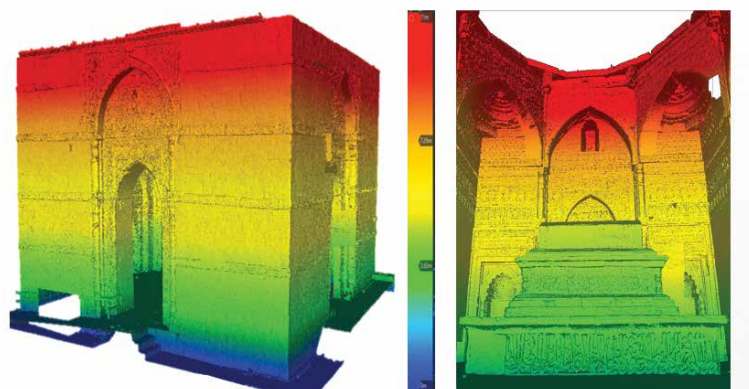


Figure 5 b: Ultra-dense laser scan of external and internal views of the tomb of Iltutmish



# ION GNSS+ 2022

**September 19-23, 2022**

Show Dates: September 21 and 22

Hyatt Regency Denver at Colorado Convention Center  
Denver, Colorado

**REGISTER TODAY**  
[ION.ORG/GNSS](https://ion.org/gnss)

# NRTK observations and their uncertainties in a modern datum

Addressing national datum modernisation, this paper presents a new approach to include static Network Real-Time Kinematic (NRTK) observations and their uncertainties in the survey control network of New South Wales (NSW), Australia.



**Tom Bernstein**  
Senior Technical Surveyor in the Metropolitan Operations & Preservation of Survey Infrastructure team at DCS Spatial Services, NSW Department of Customer Service, in Sydney, Australia



**Volker Janssen**  
Senior Technical Surveyor in the Geodetic Operations team at DCS Spatial Services, NSW Department of Customer Service, in Bathurst, Australia

The Geocentric Datum of Australia 2020 (GDA2020) is Australia's new national datum. It is defined in the International Terrestrial Reference Frame 2014 (ITRF2014; Altamimi et al., 2016) at epoch 2020.0 and based on a single, nationwide least squares network adjustment that rigorously propagates uncertainty (ICSM, 2021).

DCS Spatial Services, a unit of the NSW Department of Customer Service (DCS), is responsible for the maintenance and improvement of the state's survey control network, which comprises more than 250,000 survey marks on public record made available via the Survey Control Information Management System (SCIMS).

The backbone of the NSW survey control network is provided by CORSnet-NSW, Australia's largest state-owned and operated Global Navigation Satellite System (GNSS) Continuously Operating Reference Station (CORS) network. CORSnet-NSW currently consists of 202 stations, providing fundamental positioning infrastructure that is authoritative, accurate, reliable and easy-to-use for a wide range of applications (e.g. Janssen et al., 2016; DCS Spatial Services, 2022).

This paper describes the growing GDA2020 state adjustment and presents a new approach to include Network Real-Time Kinematic (NRTK) observations

and their Positional Uncertainty (PU) in the NSW survey control network. We exploit the automatically computed GNSS baselines between NRTK observations and their Virtual Reference Station (VRS; Landau et al., 2002) to create a connected network that can be adjusted like a static GNSS network. Using a typical urban NRTK survey in Sydney as an example, it is shown that this method offers a rigorous computation of PU while maintaining the quick and easy nature of NRTK positioning.

## GDA2020 state adjustment in NSW

Currently, the growing GDA2020 state adjustment consists of approximately 946,000 measurements between 127,000 stations, translating into about 109,000 SCIMS marks and making it the largest Jurisdictional Data Archive (JDA) in Australia. It was computed with DynAdjust using a phased-adjustment least squares methodology that provides rigorous uncertainty across the entire network (Fraser et al., 2022). The GDA2020 state adjustment includes about 114,000 GNSS baselines, 19,600 baselines originating from AUSPOS sessions, 217,000 directions and 225,000 distances. AUSPOS is Geoscience Australia's free online Global Positioning System (GPS) processing service (GA, 2022; Janssen and McElroy, 2022).

However, this only represents 43% of the 250,000 survey marks on public record in NSW, with the remaining 57% having been transformed from the now superseded GDA94 to GDA2020. Uncertainties of these transformed GDA2020 coordinates cannot be computed until the underlying measurements are sourced and readjusted with a well-defined connection to datum in the GDA2020 state adjustment. Presently, DCS Spatial Services is accelerating the process of including additional survey marks in the state adjustment to improve user access to GDA2020 coordinates and uncertainties.

To achieve this, DCS Spatial Services has developed and implemented several innovative, highly automated tools and workflows to prepare, process and ingest existing and new GNSS baseline data, AUSPOS datasets and street-corner traversing data. Over several years, efforts have been undertaken to source, harvest, clean and utilise legacy geodetic measurements (Haasdyk and Watson, 2013), build state-of-the-art GNSS CORS network infrastructure (CORSnet-NSW), observe new high-quality GNSS measurements to connect the existing survey network to CORS (Gowans and Grinter, 2013), and systematically rationalise, maintain, upgrade and collect AUSPOS datasets at key sites across the NSW survey control network, including trigonometrical (trig) stations and Australian Height Datum (AHD) spirit-levelled marks (Gowans et al., 2015; Janssen and McElroy, 2021).

Key components of these datum modernisation efforts have been the preservation and upgrade of survey infrastructure, including physical maintenance of permanent survey marks, and the update of metadata such as survey mark information in SCIMS and survey mark photographs. This will allow future users to achieve DCS Spatial Services' vision of a PU of 20 mm in the horizontal and 50 mm in the vertical (ellipsoidal height) component anywhere in the state and to easily apply transformation tools to move between current, future and various historical datums and local working surfaces.

It is worth noting that a single, state-wide levelling adjustment for NSW is currently also being generated, based on data-mining existing levelling files in the DCS Spatial Services archive and the recently digitised historical levelling data that was used to define the AHD across the state. Presently, the NSW levelling adjustment comprises about 132,000 measurements and 98,000 stations. While still underway, the enormity of this task and its benefits to the profession should not be underestimated. Victoria has already completed a state-wide levelling adjustment, and other Australian jurisdictions are now also starting similar projects.

## Determining PU for NRTK observations

Positional Uncertainty (PU) is defined as the uncertainty of the horizontal and/or vertical coordinates of a point, at the 95% confidence level, with respect to the defined datum (ICSM, 2020). It can be separated into Horizontal PU (HPU) for horizontal position and Vertical PU (VPU) for ellipsoidal height. HPU is expressed as the radius of a 95% circle of uncertainty, generally calculated from the standard error ellipse produced by a least squares network adjustment. VPU is a linear quantity and obtained by scaling the standard deviation by 1.96 to convert it to 95% confidence.

Given that NRTK observations are generally treated as point-based position solutions lacking connection to the surrounding datum, it is necessary to investigate how to propagate PU to NRTK observations and assign realistic uncertainties that can be incorporated into the GDA2020 state and national adjustments. When using CORSnet-NSW, single-base RTK positioning results can be expressed as a baseline to the CORS used and thus ingested. However, while NRTK has been shown to provide superior positioning quality compared to single-base RTK and is therefore preferable (e.g. Janssen and Haasdyk, 2011), this process is not as straightforward.

As outlined in Bernstein and Janssen (2021), we initially investigated the possibility of empirically estimating PU based on a dataset of more than 1,500 observations on more than 750 marks, collected under typical conditions encountered in surveying practice. This resulted in estimates of 0.036 m for HPU and 0.059 m for VPU. This simplistic method can be easily applied to all NRTK observations, including historical NRTK data. However, major limitations are that it provides estimated (rather than rigorously calculated) uncertainties and continues to treat NRTK observations as point-based position solutions, therefore exhibiting poor correlation with surrounding survey marks in the GDA2020 state adjustment. Furthermore, these empirical values may not always be realistic, particularly under challenging observing conditions.

Then we calculated PU individually for each NRTK observation, based on the coordinate quality (CQ) indicators provided by the GNSS equipment, resulting in overly optimistic values. While a scale factor can be applied to obtain more realistic PU values, this adds statistical guesswork to a process that was intended to be more rigorous than the empirically derived PU estimate. The varying proprietary methods of CQ computation between GNSS receiver makes and models add further complexity to the derivation of a reliable scale factor, and separate scale factors may be necessary for the horizontal and vertical components. NRTK observations continue to be treated as point-based solutions with uncertainties (poor correlation with surrounding marks), and historical data would have to be reprocessed. Consequently, this does not provide a significant advantage over the use of empirically derived values, while adding a degree of complexity.

## Generating a NRTK baseline network

NRTK observations are generally treated as point-based solutions with VRS data being discarded

after computation, which causes issues when attempting to incorporate NRTK observations and their uncertainties into a least squares network adjustment. Our new approach overcomes this issue by exploiting the automatically computed GNSS baselines between NRTK observations and their VRS to create a connected network.

Depending on fieldwork practices, multiple observations share a common VRS and are therefore linked by GNSS baselines. A VRS generally remains active until the GNSS rover is turned off or moves more than 5 km away, i.e. a typical NRTK survey usually exhibits a high degree of connectivity. These connections potentially allow PU values to be rigorously computed via least squares analysis, facilitating simple integration of NRTK data into the GDA2020 state adjustment.

While the VRS coordinates are computed from surrounding CORS data (with the CORS forming the backbone of the datum), it can be argued that the VRS itself is technically not connected to the datum. However, the VRS can be treated as a pseudo-datum station, with the connection to datum completed by deriving a baseline from each VRS to the nearest (or multiple) CORS.

Following the philosophy applied by the Intergovernmental Committee on Surveying and Mapping (ICSM) for including National GNSS Campaign Archive (NGCA) data in the national GDA2020 adjustment, a connection to the two nearest CORS is used here. It is important to note that these derived baselines are not observations, but simply joins used to connect the VRS (and thus the survey) to the datum and to transfer the uncertainty of the datum connection through to the survey network in the adjustment.

As such, this approach employs the automatically computed GNSS baselines between NRTK observations and their VRS together with a derived join between each VRS and the two nearest CORS to create a connected network that is adjustable like a traditional, static GNSS network (Figure 1).

### Putting theory into practice

We can illustrate this approach by investigating a typical urban NRTK survey conducted by DCS Spatial Services, incorporating 126 observations on 62 marks in Sydney. Best practice guidelines were followed, with each mark occupied at least twice, at least 30 minutes apart, and for a minimum of 2 minutes. Using multiple occupations on each mark adds redundancy, strengthens network geometry and helps minimise outliers. The resulting network exhibited a high degree of connectivity through the baselines automatically generated between VRS and observed mark. While the user has limited control over the network geometry created in this way, the network can be processed akin to a static GNSS survey.

In order to perform a least squares adjustment and allow this survey to influence and be influenced by the datum, it must be connected to it. In this case, six control marks that are part of the GDA2020 state adjustment were observed to provide this datum connection, leaving 56 marks to be adjusted. However, considering that a new VRS is generated when the instrument is turned off or moved more than 5 km from its original VRS location, some marks can potentially become isolated (or disconnected) from the network and datum.

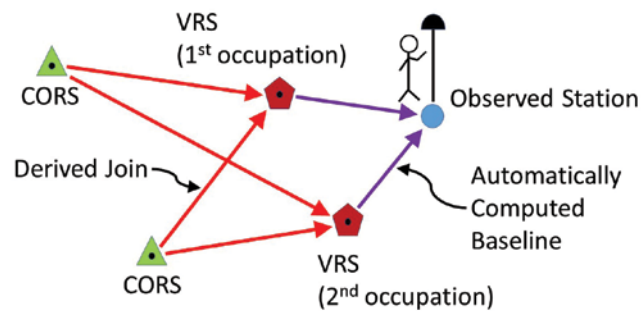


Figure 1: NRTK automatic baseline network being connected to datum via a join between each VRS and the two nearest CORS.

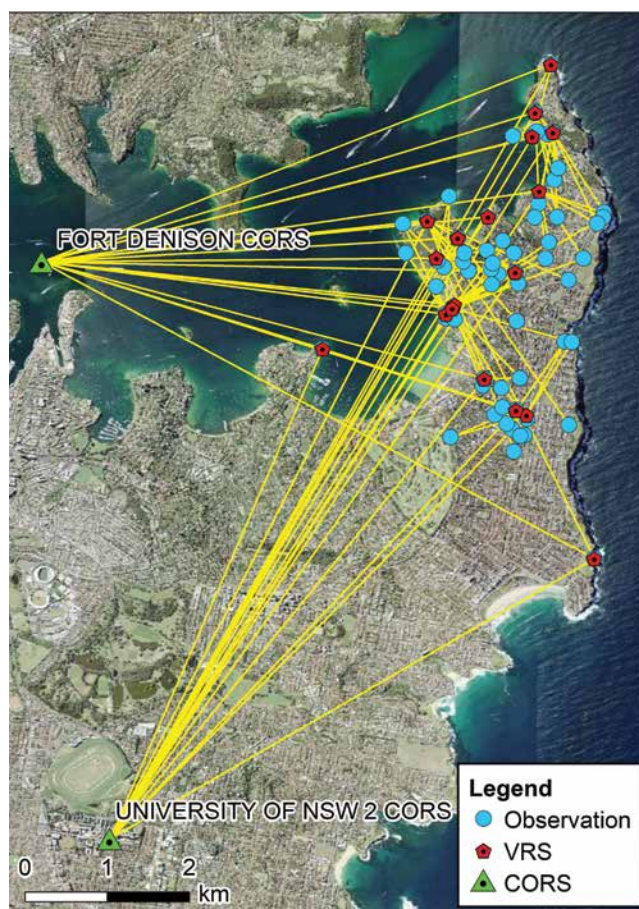


Figure 2: NRTK baseline network including the joins from each VRS to the two nearest CORS.

To ensure connection of all marks to the network, the VRS were treated as pseudo-datum stations joined to the nearest two CORSnet-NSW sites, which were then also constrained in the adjustment (Figure 2). We adjusted this survey network separately to the GDA2020 state adjustment to analyse the statistical results produced by this approach and to obtain preliminary values of PU. These PU values will be updated when this network is incorporated into the GDA2020 state adjustment.

The determination of NRTK uncertainty based on modelling the contributing errors is an ongoing area of research (e.g. Baybura et al., 2019; Ouassou and Jensen, 2019; Jongrujan and Satirapod, 2020). In this case, baseline weightings were chosen to mimic the standard deviation values ( $1\sigma$ ) routinely applied by DCS Spatial Services for NRTK uncertainty in practice: 0.014 m (horizontal) and 0.030 m (vertical). These values include allowance for to/from centring errors and have proven realistic in most practical observing conditions using

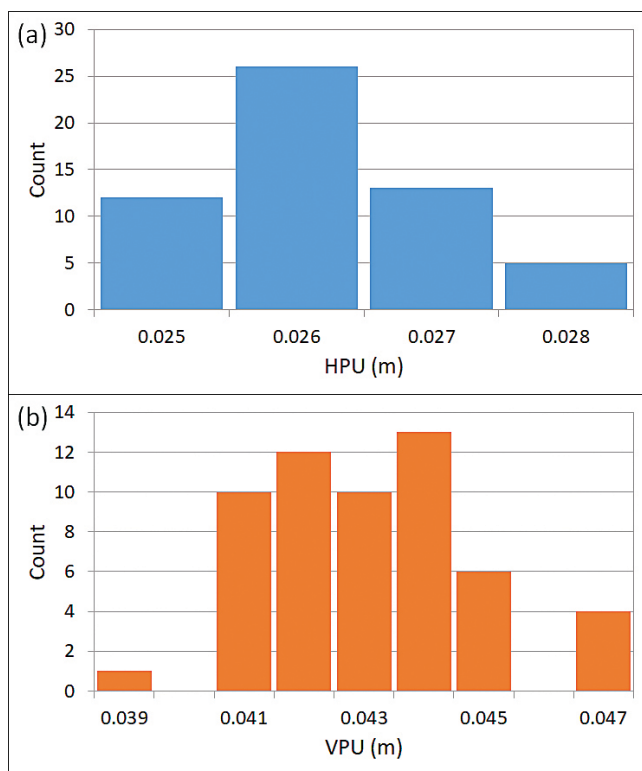


Figure 3: Calculated (a) HPU and (b) VPU for NRTK observations based on the NRTK baseline network.

Table 1: Descriptive statistics for HPU and VPU, calculated based on the NRTK baseline network for 56 adjusted marks (all values in metres).

Descriptive Statistic	HPU	VPU
Minimum	0.025	0.039
Maximum	0.028	0.047
Mean	0.026	0.043
Median	0.026	0.043
Standard Deviation	0.001	0.002

CORSnet-NSW. While it is known that NRTK observations exhibit a small degree of distance dependency, recent studies have found no significant effect for NRTK solutions located up to 40-50 km from the nearest CORS (Gökdas and Özlüdemir, 2020). Consequently, residual NRTK distance dependency can be ignored in this case.

Since each observation is connected to the datum by two baselines (i.e. CORS to VRS and VRS to occupied mark) and to avoid inflation of the uncertainties through this join in the adjustment, these initial values were divided by  $\sqrt{2}$  according to the error propagation law. This resulted in final weightings of 0.010 m (horizontal) and 0.021 m (vertical) for each baseline, with no distance dependency applied.

As previously mentioned, the two CORS served as constraints in the fully constrained adjustment, along with the six GDA2020 control marks that braced the network. The median HPU of these eight constraints was 0.018 m, and the median VPU was 0.026 m. The adjustment achieved a variance factor of 0.9, which is expected for a network of this nature. In this case, as a business rule, DCS Spatial Services does not tighten the input standard deviations to achieve a variance factor of unity. Histograms of the resulting PU values are shown in Figure 3, while corresponding descriptive statistics are summarised in Table 1.

The adjustment provided individual uncertainties for each NRTK observation, with median values of 0.026 m (HPU) and 0.043 m (VPU), i.e. about 0.010 m and 0.015 m better than the empirical estimates obtained earlier. This can be explained by improved geometry and redundancy due to the network adjustment. These preliminary results demonstrate the appropriateness of the observational weighting strategy used and that this method can provide reliable results. Current work investigates tweaking the observational weighting strategy to optimise the inclusion of NRTK observations with realistic uncertainties in the GDA2020 state adjustment.

## Conclusion

Australia’s new national datum, GDA2020, is based on a single, nationwide least squares network adjustment that rigorously propagates uncertainty. As the GDA2020 state adjustment continues to grow, efforts are underway at DCS Spatial Services to further increase user access to Positional Uncertainty for survey marks on public record in NSW.

This paper has described the GDA2020 state adjustment and presented a new approach to include NRTK observations and their PU in the NSW survey control network via the GDA2020 state adjustment. We employed the automatically computed baselines between NRTK observations and their VRS, combined with a derived join between each VRS and the two nearest CORS, to create a connected network that can be adjusted akin to a static GNSS network. Using a typical urban NRTK survey in Sydney as an example, PU was calculated to be about 0.026 m (HPU)

---

Australia's new national datum, GDA2020, is based on a single, nationwide least squares network adjustment that rigorously propagates uncertainty. As the GDA2020 state adjustment continues to grow, efforts are underway at DCS Spatial Services to further increase user access to Positional Uncertainty for survey marks on public record in NSW.

---

and 0.043 m (VPU), comparing reasonably well to empirical positioning quality and user experience.

This approach provides a rigorous method of computing realistic PU and allows easy integration into the GDA2020 state adjustment, while maintaining the quick and easy nature of NRTK positioning. These benefits come at no expense to fieldwork time or complexity. The processing load is only marginally increased (network adjustment rather than site transformation), once CORS-to-VRS baseline derivation is automated. The need for each historical NRTK survey to be adjusted separately is a reasonable price to pay for this comprehensive solution.

Adoption of this methodology will allow NRTK data to be rigorously included in the GDA2020 state adjustment, enabling DCS Spatial Services to further maintain and improve the NSW survey control network for the benefit of all.

## References

- Altamimi Z., Rebischung P., Métivier L. and Collilieux X. (2016) ITRF2014: A new release of the International Terrestrial Reference Frame modelling nonlinear station motions, *Journal of Geophysical Research: Solid Earth*, 121(8), 6109-6131.
- Baybura T., Tiryakioglu I., Ugur M.A., Solak H.I. and Safak S. (2019) Examining the accuracy of Network RTK and long base RTK methods with repetitive measurements, *Journal of Sensors*, 2019, 3572605, <https://doi.org/10.1155/2019/3572605>.
- Bernstein T. and Janssen V. (2021) Positional Uncertainty of Network RTK observations in a modern datum, *Journal of Geodetic Science*, 11(1), 38-47.
- DCS Spatial Services (2022) CORSnet-NSW, <http://www.corsnet.com.au/> (accessed Aug 2022).
- Fraser R., Leahy F. and Collier P. (2022) DynAdjust user's guide, version 1.2, <https://github.com/icsm-au/DynAdjust/tree/master/resources> (accessed Aug 2022).
- GA (2022) AUSPOS – Online GPS processing service, <http://www.ga.gov.au/scientific-topics/positioning-navigation/geodesy/auspos> (accessed Aug 2022).
- Gökdas Ö. and Özlüdemir M.T. (2020) A variance model in NRTK-based geodetic positioning as a function of baseline length, *Geosciences*, 10(7), 262, <https://doi.org/10.3390/geosciences10070262>.
- Gowans N. and Grinter T. (2013) Tying it all together: CORSnet-NSW local tie surveys, *Proceedings of Association of Public Authority Surveyors Conference (APAS2013)*, Canberra, Australia, 12-14 March, 104-119.
- Gowans N., McElroy S. and Janssen V. (2015) Survey infrastructure preservation and upgrade: Trigonometrical stations in NSW, *Proceedings of Association of Public Authority Surveyors Conference (APAS2015)*, Coffs Harbour, Australia, 16-18 March, 67-84.
- Haasdyk J. and Watson T. (2013) Data-mining in NSW: Towards a new and improved Australian datum, *Proceedings of Association of Public Authority Surveyors Conference (APAS2012)*, Canberra, Australia, 12-14 March, 85-102.
- ICSM (2020) Standard for the Australian survey control network (SP1), version 2.2, <https://www.icsm.gov.au/publications/standard-australian-survey-control-network-special-publication-1-sp1> (accessed Aug 2022).
- ICSM (2021) Geocentric Datum of Australia 2020 technical manual, version 1.7, <https://www.icsm.gov.au/gda2020-and-gda94-technical-manuals> (accessed Aug 2022).
- Janssen V. and Haasdyk J. (2011) Assessment of Network RTK performance using CORSnet-NSW, *Proceedings of IGNSS Symposium 2011 (IGNSS2011)*, Sydney, Australia, 15-17 November, 18pp.
- Janssen V., Haasdyk J. and McElroy S. (2016) CORSnet-NSW: A success story, *Proceedings of Association of Public Authority Surveyors Conference (APAS2016)*, Leura, Australia, 4-6 April, 10-28.
- Janssen V. and McElroy S. (2021) Australian Height Datum: Saving AHD in New South Wales, *Coordinates*, 17(6), 6-10.
- Janssen V. and McElroy S. (2022) A practical guide to AUSPOS, *Proceedings of Association of Public Authority Surveyors Conference (APAS2022)*, Leura, Australia, 21-23 March, 3-28.
- Jongrujan T. and Satirapod C. (2020) Stochastic modeling for VRS network-based GNSS RTK with residual interpolation uncertainty, *Journal of Applied Geodesy*, 14(3), 317-325.
- Landau H., Vollath U. and Chen X. (2002) Virtual reference station systems, *Journal of Global Positioning Systems*, 1(2), 137-143.
- Ouassou M. and Jensen A.B.O. (2019) Network real-time kinematic data screening by means of multivariate statistical analysis, *SN Applied Sciences*, 1(6), 512, <https://doi.org/10.1007/s42452-019-0531-3>. 



# New insights into large tropical tree mass and structure from direct harvest and Terrestrial Lidar

In this paper, we present, to our knowledge, the first validation of Lidar-derived AGB estimates of tropical trees using reference values obtained entirely from direct measurement

## Andrew Burt

Department of  
Geography, University  
College London,  
London, UK

## Matheus Boni Vicari

Department of  
Geography, University  
College London,  
London, UK

## Antonio C. L. da Costa

Instituto de Geosciências,  
Universidade Federal  
do Pará, Belém, Brazil

## Ingrid Coughlin

Research School of  
Biology, Australian  
National University,  
Canberra, Australia

## Patrick Meir

Research School of  
Biology, Australian  
National University,  
Canberra, Australia  
School of GeoSciences,  
University of Edinburgh,  
Edinburgh, UK

## Lucy Rowland

College of Life and  
Environmental  
Sciences, University  
of Exeter, Exeter, UK

## Mathias Disney

Department of  
Geography, University  
College London, London,  
UK  
NERC National Centre  
for Earth Observation  
(NCEO), Leicester, UK

## Abstract

A large portion of the terrestrial vegetation carbon stock is stored in the above-ground biomass (AGB) of tropical forests, but the exact amount remains uncertain, partly owing to the lack of measurements. To date, accessible peer-reviewed data are available for just 10 large tropical trees in the Amazon that have been harvested and directly measured entirely via weighing. Here, we harvested four large tropical rainforest trees (stem diameter: 0.6–1.2 m, height: 30–46 m, AGB: 3960–18 584 kg) in intact old-growth forest in East Amazonia, and measured above-ground green mass, moisture content and woody tissue density. We first present rare ecological insights provided by these data, including unsystematic intra-tree variations in density, with both height and radius. We also found the majority of AGB was usually found in the crown, but

varied from 42 to 62%. We then compare non-destructive approaches for estimating the AGB of these trees, using both classical allometry and new lidar-based methods. Terrestrial lidar point clouds were collected pre-harvest, on which we fitted cylinders to model woody structure, enabling retrieval of volume-derived AGB. Estimates from this approach were more accurate than allometric counterparts (mean tree-scale relative error: 3% versus 15%), and error decreased when up-scaling to the cumulative AGB of the four trees (1% versus 15%). Furthermore, while allometric error increased fourfold with tree size over the diameter range, lidar error remained constant. This suggests error in these lidar-derived estimates is random and additive. Were these results transferable across forest scenes, terrestrial lidar methods would reduce uncertainty in stand-scale AGB estimates, and therefore advance our understanding of the role of tropical forests in the global carbon cycle.

## 1. Introduction

Forests in Amazonia are estimated to store in the region of 50–60 Pg of carbon in above-ground live vegetation [1–3], and are probably a small carbon sink, estimated at  $0.25 \pm 0.3 \text{ Pg C yr}^{-1}$ , but appear to be trending towards becoming a carbon source [4]. The uncertainty in these values has implications for policy assessment: commensurate uncertainty exists in the exact benefits provided by afforestation and reforestation programmes (e.g.

REDD+ or carbon trading schemes), or likewise, the expediency of deforestation.

The cornerstone of any Amazon-scale estimate of carbon stocks are the networks of calibration sites; censused forest stands where the above-ground biomass (AGB; i.e. the mass of above-ground live plant matter at 0% moisture content) of each tree has been quantified (the carbon content of biomass varies, but is often observed between 45–50%) [5–7]. However, there is not a single hectare of tropical forest on Earth whose AGB has been directly measured. At these calibration sites then, measurements are replaced with estimates.

This is because directly measuring the AGB of a tree is resource intensive: it requires the tree to be harvested, and subsequent measurement of: (i) above-ground green mass via weighing, and (ii) the moisture content of this green mass. Indeed, we could find just 10 large tropical trees (stem diameter  $\geq 0.6$  m) in Amazonia whose above-ground green mass had been directly measured and recorded in the peer-reviewed English language literature, where data were enumerated [8]. This increased to 60 when direct weighing measurements of above-ground green mass were at least partially replaced with geometry-derived volume estimates [9–14].

In the absence of measurements, AGB must instead be estimated at these calibration sites using allometry [15]. Allometric models describe the correlations that exist between tree-scale AGB, and more readily measured tree variables (e.g. stem diameter). These models are constructed, usually via log-transformed linear regression, using calibration (in-sample) data collected from destructively harvested trees, where AGB was measured concurrent with these predictor variables. For tropical forests, calibration data are usually collected from across the region or population (i.e. Amazonia or pan-tropics), rather than more locally by either geography or taxa, owing to diversity [16]. Widely used pan-tropical allometric models also include additional predictor variables

beyond stem diameter, such as tree height and wood density, partly to reduce the standard error of the regression (i.e. these variables are correlated with AGB), and partly to enable capture of systematic biogeographic variations in tree height and wood density [17–19].

Error in allometric estimates potentially arises from the selection, measurement and modelling of the calibration data, as well as from the measurement of the out-of-sample data (i.e. the predictor variables of the tree whose AGB is to be estimated). A trait of allometric error is that it is multiplicative: that is, it is well observed that variance in AGB is not constant across tree size (i.e. variance in AGB increases with increasing stem diameter and tree height; heteroscedasticity), therefore error itself increases with tree size [20]. At the tree-scale then, uncertainty in an allometric estimate of AGB is proportional to tree size, and it has been demonstrated that in tropical forests, it is possible for uncertainty to be larger than the estimate itself [21]. At the 1 ha stand-scale, random errors begin to average out, but it would still be reasonable to expect uncertainty to remain upwards of 40% [22]. Furthermore, unquantifiable systematic error probably increases these uncertainties further, regardless of scale, because of, among various reasons, imbalances in widely used calibration data, which are typically skewed toward smaller trees [23]. In absolute terms then, uncertainty in current state-of-the-art estimates of stand-scale AGB is potentially large, and relatively, a function of stand composition. Such uncertainties at the aforementioned calibration sites are of concern because they propagate directly through to larger-scale estimates of AGB and carbon stocks [24].

Recently, a new alternative method for estimating tree- and stand-scale AGB has been pioneered using terrestrial lidar data [25]. Modern terrestrial laser scanners enable capture of rich-but-unorganized point clouds that provide a millimetre-accurate three-dimensional sample of observable elements in forest scenes. Current hardware and data

acquisition protocol enable high-quality data to be collected from, for example, a 1 ha tropical forest stand within a week of scanning [26]. Various tools and workflows have been developed to process these data: from the segmentation of point clouds representing individual trees, the classification of individual points as returns from either wood or leaf surfaces, to the construction of quantitative structural models (QSMs) via shape fitting, to explicitly describe woody tree architecture [27–31]. Together, these methods enable retrieval of above-ground green woody volume from lidar data that, combined with a value of density, permit estimation of tree-scale AGB (note: these estimates of volume are derived from sampling external woody surfaces, so they are unable to account for either internal rot/cavities, or the contribution of leaf material to volume).

It is important at this point to briefly introduce the value of density required to convert these lidar-derived volumes into estimates of AGB. Throughout this paper, we use the rather cumbersome term ‘above-ground basic woody tissue density’, because the value is required to have the following three properties. First, the lidar data provide a three-dimensional sample of any particular tree in a green state (i.e. it is assumed cell walls are saturated, and lumina filled with water), so to estimate dry mass from green volume, a basic density (i.e. dry mass over green volume) is required. Second, this single value must account for the density of each above-ground woody tissue (i.e. periderm, phloem, cambium, xylem and pith) filling the volume, weighted by the relative abundance of each tissue. Third, this value must account for the intra-tree variations in the density of these tissues, which have been observed to vary with both radius and height [32,33].

The fundamental attraction of this lidar-based approach, over classical allometry, is that AGB estimates are not derived from calibration data collected from other, unrelated trees, but from explicit three-dimensional measurements of the particular tree itself. Additionally,

the various processing methods (e.g. shape fitting) for estimating above-ground green woody volume are scale invariant, and therefore in an idealized scenario, there is no expectation for error in these estimates to be correlated with tree size; that is, error is additive. This is a potentially important differentiator between lidar- and allometric-based approaches, because it would mean that when these lidar-derived estimates are up-scaled, the error in stand-scale estimates would be independent of the stand and its composition. However, the question remains: what is the error, both random and systematic, in these estimates? While there are different approaches to answering this question, including simulation experiments, the gold standard is to compare estimates,  $AGB_{est}$ , with directly measured reference values,  $AGB_{ref}$ .

To date, several publications present studies validating  $AGB_{est}$  retrieved from terrestrial lidar data via QSM-derived volume estimates. Calders et al. [34] collected both lidar and destructive measurements from 65 trees in *Eucalyptus* spp. open forest in Australia, and using their particular lidar data processing chain, found the coefficient of variation of the root mean square error in tree-scale  $AGB_{est}$  to approximate 16%. Perhaps the most significant finding was the absence of a correlation between error and tree size, which provided the first empirical evidence to support the aforementioned hypothesis that error in these estimates is additive. For tropical forests, Momo et al. [35] acquired lidar and destructive data in Cameroon for 61 trees (mean stem diameter: 0.58 m, tree height: 34 m), and found the mean tree-scale relative error in  $AGB_{est}$  approximated 23%. Gonzalez de Tanago et al. [36] also collected similar data in Guyana, Indonesia and Peru for 29 trees (mean stem diameter: 0.73 m), and found the coefficient of variation of the root mean square error in tree-scale  $AGB_{est}$  to approximate 28%. In contrast to [34], error was observed to increase with tree size in both these studies. One possible explanation for this, and the overall increase in error, is the additional difficulty in acquiring

high-quality lidar and destructive data in dense and remote tropical forests.

For example, in both [35,36],  $AGB_{ref}$  could not always be obtained from direct measurements of green mass. Instead, for all trees [36], or for portions of large trees [35], mass was instead estimated from geometry: length and diameter measurements were converted into green volume estimates by assuming underlying tree structure could be represented by either a cylinder or conical frustum. Estimates of dry mass were then generated using an estimate of basic woody tissue density obtained from either the harvested trees themselves [35], or from a global database [36]. That is, despite the significant advances both studies achieved, both were also limited by the inability to determine how accurately  $AGB_{ref}$  represented true  $AGB$ .

In this paper, we present, to our knowledge, the first validation of lidar-derived  $AGB$  estimates of tropical trees using reference values obtained entirely from direct measurement. We decided to focus the experiment on collecting high-quality and detailed measurements from a small sample of large trees, as opposed to collecting lower quality data from a larger sample. This approach provides the opportunity to generate a robust understanding of the minimum error that can be expected in lidar-derived  $AGB$  estimates, with currently available hardware and data processing methods. Overall, we harvested four large tropical rainforest trees (stem diameter range: 0.6–1.2 m, tree height range: 30–46 m) in an intact old-growth forest stand in East Amazonia, and weighed their above-ground green mass. We also gathered multiple discs from the stem and crown of each tree, on which moisture content and woody tissue density were measured. Terrestrial lidar measurements were collected from the four trees pre-harvest using a high-performance laser scanner after neighbouring trees and understory were cleared to minimize occlusion. Tree-scale  $AGB_{est}$  was then retrieved from these data using a replicable and open-source processing chain. Crucially, these

methods rely solely on the lidar data themselves for calibration (i.e.  $AGB_{est}$  was not a priori informed by  $AGB_{ref}$ ).

In the results section, we first present the reference data from the destructive measurements. This includes rare and interesting ecological insights provided by these data, including, for each tree, the moisture content and the distribution of mass between stem and crown, as well as the intra-tree variations in basic woody tissue density. We then present the lidar data, and quantify the error in  $AGB_{est}$  retrieved from these data. We show how these errors compare with those arising from allometry. We then discuss the wider implications of these results for improving tropical forest tree- and stand-scale  $AGB$  estimates and related ecological understanding.

## 2. Methods

Destructive and non-destructive data were collected from four trees (designated T1–T4, pictured in figure 1) in Floresta Nacional de Caxiuanã, Pará, Brazil, during September and October 2018. These data are open-access and distributed under the terms of the Creative Commons Attribution 4.0 International Public License (CC BY 4.0). Persistent identifiers for these data are available in the data accessibility section.

### 2.1. Site metadata

The approximate coordinates of the site in the WGS-84 datum are  $-1.798^\circ$ ,  $-51.435^\circ$ . The site is classified as moist, terra firme, pre-quaternaly, lowland, mixed species, old-growth, intact tropical forest. Mean annual rainfall is 2000–2500 mm, with a dry season between June and November. Soils at a nearby long-term through-fall exclusion experiment (approx. 7 km from the site) are yellow oxisol, composed of 75–83% sand, 12–19% clay and 6–10% silt [37,38].

### 2.2. Tree selection

We determined tree selection should principally ensure there was some

range in the values of stem diameter and tree height. Other considerations influencing selection was a bias towards those that appeared healthy and with a complete crown, felling (in particular, that no large neighbouring trees would affect felling operations), and also permission from the land owners. The four selected trees were identified to species, and foliage/fruit samples retained to confirm taxonomic identity at the Museu Paraense Emílio Goeldi, Belem, Pará, Brazil. Nearby vegetation surrounding each tree was removed, including complete clearing of small bushes and saplings, to enable detailed non-destructive and destructive activities.

### 2.3. Non-destructive measurements

Stem diameter was measured using a circumference/diameter tape. Measurement was made at either 1.3 m above-ground (T4), or 0.5 m above-buttress (T1–T3). Lidar data were collected using a RIEGL VZ-400 terrestrial laser scanner. A minimum of 16 scans (upright and tilt) were acquired from eight scan positions around each tree, with a variable distance between scanner and tree. This arrangement provided a 45° sampling arc around each

tree, and a complete sample of the scene from each position. The angular step between sequentially fired pulses was 0.04°. The laser pulse has a wavelength of 1550 nm, a beam divergence of 0.35 mrad, and the diameter of the footprint at emission is 7 mm. The instrument was in ‘High-Speed Mode’ (pulse repetition rate: 300 kHz), ‘Near Range Activation’ was off (minimum measurement range: 1.5 m), and waveforms were not stored.

### 2.4. Destructive measurements

The various field and laboratory measurements are described below. Included in the destructive dataset are photographs illustrating these measurements.

#### 2.4.1. Field measurements

The location, height and above-ground green mass of the four trees were measured in the field, and multiple discs were also collected from each tree. Trees were cut at a height of approximately 1 m above-ground, and felled onto tarpaulin. A STIHL MS 650 chainsaw with a 20” bar length and 13/64” chain loop was used for cutting. Tree height (including stump) was then measured

with a surveyor’s tape measure, and GPS data were acquired from the centre of the stump using a Garmin GPSMAP 64st.

Two Adam LHS 500 crane scales (capacity: 500 kg, division: 0.1 kg) were suspended from nearby trees to measure green mass. Calibration certificates are included in the destructive dataset certifying both instruments conformed (pre-delivery) to various tests of repeatability, linearity and hysteresis. Post-campaign, the consistency of measurements between both scales was tested using a variety of different masses, and measurements were also compared against the laboratory balance with internal calibration weights described in the following subsection.

Green mass was assigned to either the stem or crown pool, where the stem was defined as the bole from flush with the ground up to the first fork. The stem was cut into manageable sections, the length and diameter of each section was measured using a circumference/diameter tape (lengths varied from 0.15–0.54 m for T2 and T4, respectively), and then weighed. Remaining stump material was cut flush with the ground and weighed. Large branches were cut into manageable sections, and fine branching and leaf material were collected in large sacks, and weighed. These green mass measurements commenced immediately post-felling, but two, four, four and two days were required to complete measurement of T1–T4, respectively.

Discs of approximately 50 mm thickness were collected from the stem and crown of each tree. Four discs were collected from the stem: at 1.3 m above-ground, and at 25%, 50% and 75% the length of the stem. Up to three discs were also collected from the mid-points of first, second and third-order branches. A minimum of 11 discs were collected per tree. Figure 2 shows the discs collected from T4.

#### 2.4.2. Laboratory measurements

Discs were reduced to subsamples using a consistent approach: for any particular

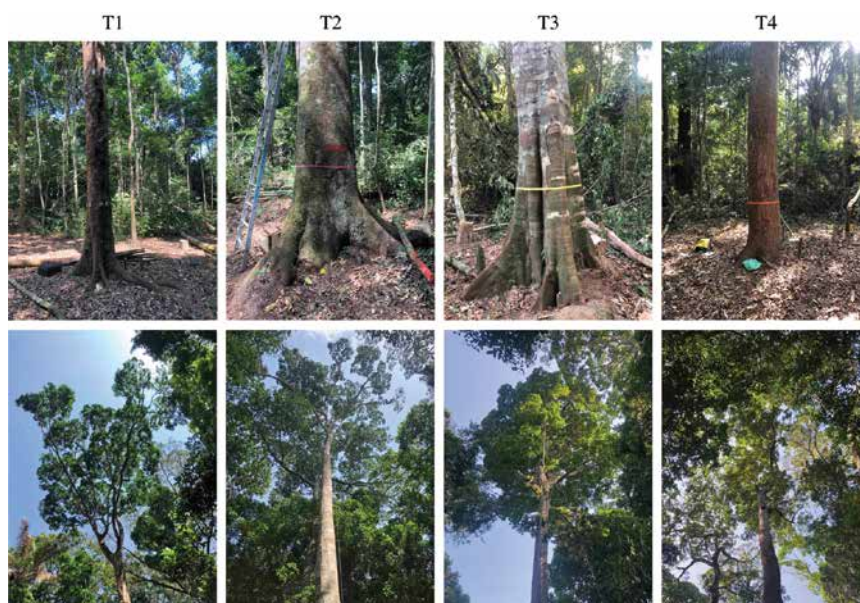


Figure 1. Photographs of the stem and crown of each harvested tree. Left to right: T1 (*Inga alba* (Sw.) Willd.), T2 (*Hymenaea courbaril* L.), T3 (*Tachigali paniculata* var. *alba* (Ducke) Dwyer) and T4 (*Trattinnickia burserifolia* Mart.).

disc, they were taken from along the major axis, as guided by parallel chords straddling above and below the length of this axis, each with approximate dimensions of 150 × 50 × 50 mm. That is, each set of subsamples covered the length of their respective disc (i.e. included periderm, phloem, cambium, xylem and pith tissues). Figure 2 also shows the sets of subsamples cut from the discs of T4.

The mass and volume of each subsample was measured while in both a green and dry state. These measurements were made using an Adam NBL4602i Nimbus Precision balance (capacity: 4600 g, division: 0.01 g). This balance contains internal calibration weights,

and a calibration certificate is available in the harvest dataset certifying this instrument conformed (pre-delivery) to external tests of repeatability, eccentric loading, linearity and hysteresis. Volume measurements were made using the balance via Archimedes' principle. Subsamples were considered in a green state after soaking for 48 h. They were considered in a dry state once a constant mass had been attained while drying in an oven at 105°C.

In the original campaign, the green volume of subsamples was not measured (necessary for calculating basic woody tissue density). We returned to the harvest site in October 2019 and collected new

discs and subsamples from the wood piles of each tree using the methods described above. The integrity of the wood was verified by comparing measurements of woody tissue green-to-dry mass ratio and dry woody tissue density. The green volume of the original subsamples was retrospectively calculated using the mean woody tissue green-to-dry volume ratio from these new subsamples.

## 2.5. Above-ground biomass

### 2.5.1. Woody tissue green-to-dry ratios and density

Above-ground woody tissue green-to-dry mass and volume ratios were estimated for each tree from measurements on the subsamples using a mass-weighted approach. These two variables were calculated by weighting the mean from the subsamples in each pool (stem and crown), with the green mass in each pool. Above-ground basic woody tissue density was estimated using three approaches: (i) mass-weighted; (ii) stem, which was calculated from the mean of the two outer subsamples taken from the stem disc at 1.3 m above-ground; and (iii) literature, where values were taken from the Global Wood Density Database [39], whereby the value considered was the mean of matched species-level entries. The second approach was intended to mimic values acquired via increment boring (i.e. a regular wood density measurement), and the third approach was considered because it is widely applied in non-destructive settings.

### 2.5.2. Reference values

$AGB_{ref}$  was calculated from measured above-ground green mass and the mass-weighted estimate of above-ground woody tissue green-to-dry mass ratio. Mass lost in swarf from chainsaw cuts was partially accounted for using a volume-derived approach (stem only). A green cut volume was estimated for each of the manageable stem sections by assuming it could be represented by a cylinder. An average cut width of 8.4 mm (approx. 60% thicker than the chain loop) was estimated from multiple



Figure 2. The photograph on the left shows the discs collected from T4. Four were acquired from the stem, at 1.3 m above-ground, and at 25%, 50% and 75% the length of the stem. Eight were taken from the mid-points of first-, second- and third-order branches. Each disc was subsequently reduced to a set of subsamples using a consistent approach: for any particular disc they were taken from along the major axis, as guided by parallel chords straddling above and below the length of this axis (upper right photograph). The lower right photograph shows all subsamples from T4. It is noted that each set of subsamples cover the full length of their corresponding disc, and therefore each set includes periderm, phloem, cambium, xylem and pith tissues.

caliper measurements. Lost dry mass was estimated from these green volumes using the mass-weighted estimates of above-ground green woody tissue density and above-ground woody tissue green-to-dry mass ratio. These corrections increased  $AGB_{ref}$  by 0.7%, 1.8%, 0.7% and 0.7% for T1–T4, respectively.

### 2.5.3. Lidar-derived estimates

Estimates of above-ground green woody volume were retrieved from the lidar data using the software described below. With the exception of the initial step, these tools are open-source, and persistent identifiers for the source code are available in the data accessibility section. Individual lidar scans were registered onto a common coordinate system using RiScan Pro (v. 2.7.0) [40]. The point clouds representing the individual trees were extracted from the larger-area point clouds using TreeSEG (v. 0.2.0) [28]. Returns from leafy surfaces were segmented from these tree-level point clouds after wood-leaf classification using TLSeparation (v. 1.2.1.5) [27]. Points from buttresses were then manually removed using CloudCompare (v. 2.10.3) [41]. QSMs were constructed from these point clouds using TreeQSM (v. 2.3.2) [31]. Input parameters to TreeQSM were automatically selected using optQSM (v. 0.1.0).  $AGB_{est}$  was calculated from estimated above-ground green woody volume and the mass-weighted estimate of above-ground basic woody tissue density.

### 2.5.4. Allometric-derived estimates

$AGB_{est}$  was calculated using the two-parameter model described in Chave *et al.* [11] (eqn (4), three predictor variables: stem diameter,  $D$  (cm), tree height,  $H$  (m) and basic wood density,  $\rho$  (g cm<sup>-3</sup>). This model is constructed from measurements collected on 4004 destructively harvested trees from across the tropics, and takes the form:

$$AGB_{est} \approx 0.067(D^2 H \rho)^{0.976}, \quad 2.1$$

where here, stem diameter was measured pre-harvest using a circumference/diameter tape at 1.3 m above-ground (T4) or 0.5 m above-buttress (T1–T3), tree height was measured post-harvest using a surveyor's tape measure, and basic wood density was represented by the mass-weighted estimate of above-ground basic woody tissue density. The electronic supplementary material, appendix A considers our decision to select this particular model to represent the allometric approach.

### 2.5.5. Estimate performance

To describe the performance of lidar- and allometric-derived  $AGB_{est}$ , we use the terms random error, systematic error, total error, precision, trueness, accuracy, bias and uncertainty. For the avoidance of doubt, these terms are used within the International Organization for Standardization 5725 and the International Bureau of Weights and Measures definitions [42]. Error,  $\epsilon$ , in  $AGB_{est}$  is defined as

$$\epsilon = AGB_{est} - AGB_{ref}. \quad 2.2$$

Relative error is defined as

$$RE = \frac{|\epsilon|}{AGB_{ref}}. \quad 2.3$$

Mean tree-scale relative error is defined as

$$MRE = \frac{1}{n} \sum_{i=1}^n RE_i. \quad 2.4$$

Mean error is used to quantitatively express trueness:

$$ME = \frac{1}{n} \sum_{i=1}^n \epsilon_i. \quad 2.5$$

The standard deviation of the error is used to quantitatively express precision:

$$STDEV = \sqrt{\frac{1}{n} \sum_{i=1}^n (\epsilon_i - \bar{\epsilon})^2}. \quad 2.6$$

Root mean square error is used to quantitatively express accuracy:

$$RMSE = \sqrt{\frac{1}{n} \sum_{i=1}^n \epsilon_i^2}. \quad 2.7$$

## 3. Results

### 3.1. Ecological insights from the harvest measurements

Directly measured above-ground green mass of the four trees ranged from 6808 to 29 511 kg, totalling 59 005 kg (table 1).

**Table 1. Variables of the four harvested trees. (The approach to each measurement is described in the methods section. It is noted that conversion of above-ground green mass to above-ground dry mass via above-ground woody tissue green-to-dry mass ratio does not yield the reported value. This is because above-ground dry mass includes a correction to partially compensate for mass lost in swarf from chainsaw cuts. These corrections were 27.7 kg, 330.2 kg, 58.1 kg and 41.0 kg for T1–T4, respectively.)**

ID	species	coords (°)	$D$ (m)	$H$ (m)	above-ground green mass (kg)	above-ground dry mass ( $AGB_{ref}$ ) (kg)	above-ground basic woody tissue density (kg m <sup>-3</sup> )			above-ground woody tissue green-to-dry ratio	
							mass-weighted	stem	literature	mass	volume
T1	<i>Inga alba</i> (Sw.)	– 1.79851	0.647	29.8	6808.2	3960.1	567.6	574.6	586.1	1.731	1.169
	Willd.	– 51.43463									
T2	<i>Hymenaea</i>	– 1.79832	1.179	46.2	29511.0	18584.2	768.9	786.7	792.4	1.617	1.126
	<i>courbaril</i> L.	– 51.43479									
T3	<i>Tachigali paniculata</i> var.	– 1.79914	0.905	34.9	13697.5	8392.6	639.0	655.1	554.5	1.643	1.137
	<i>alba</i> (Ducke) Dwyer	– 51.43451									
T4	<i>Trattinnickia</i>	– 1.79550	0.697	35.2	8988.6	5521.1	567.0	561.9	460.0	1.640	1.113
	<i>burserifolia</i> Mart.	– 51.43433									

The disc-derived mass-weighted estimates of above-ground woody tissue green-to-dry mass ratio ranged from 1.62 to 1.73, implying that in the region of 40% of this green mass was water.  $AGB_{ref}$  calculated from the above values, ranged from 3960 to 18 584 kg, totalling 36 458 kg. The proportion of  $AGB_{ref}$  distributed between the stem and crown varied between trees, with the crown mass ratio ranging from 0.42 to 0.62, but for three out of four, the majority was found in the crown (figure 3).

The mass-weighted estimates of above-ground basic woody tissue density ranged from 568 to 769  $kg\ m^{-3}$  for the four trees. Values generated from the other direct approach using the discs (stem), which were intended to mimic measurements acquired via increment boring, were consistent with mass-weighted counterparts, with a maximum percentage difference of 2% (table 1 and figure 4). Non-direct values obtained from the literature were less consistent: for T1 and T2 they were close, but were significantly lower than mass-weighted estimates in both T3 and T4, with a percentage difference of 3%, 3%, 14% and 20% for T1–T4, respectively.

Beneath these whole-tree values were substantial and unsystematic intra-tree variations in basic woody tissue density (figure 4). Overall, density decreased with height in T2, increased in T3 and T4, and remained largely invariant in T1. A pronounced decrease was also observed towards the centre of each stem disc in T3, which was not seen in the other trees. The maximum difference between measurements on the subsamples collected throughout each tree was 40  $kg\ m^{-3}$ , 79  $kg\ m^{-3}$ , 166  $kg\ m^{-3}$  and 156  $kg\ m^{-3}$  for T1–T4, respectively.

### 3.2. Non-destructive above-ground biomass estimates

The downsampled terrestrial lidar data comprised a minimum 2.6 million points per tree (figure 3). The QSMs constructed from

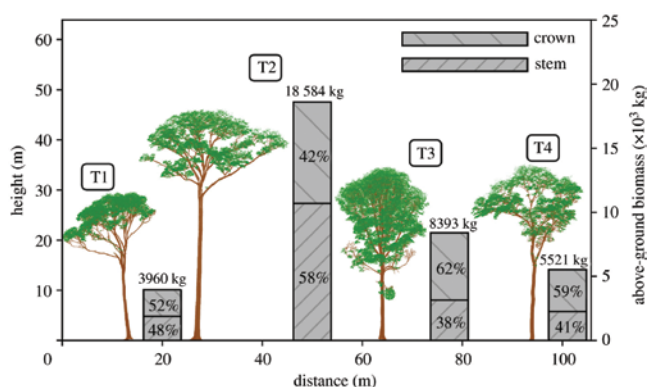


Figure 3. The terrestrial lidar point clouds collected from the four trees prior to harvest. Shown to scale, left to right: T1–T4. These clouds were segmented from the larger-area point clouds using TreeSEG [28], and individual points were classified as returns from wood (brown) and leaf (green) surfaces using TLSeparation [27]. The bars on the secondary y-axis provide the harvest-derived reference values of above-ground biomass ( $AGB_{ref}$ ). Also shown in these bars are the distributions of  $AGB_{ref}$  between the stem and crown.

the woody point clouds are shown in figure 5.  $AGB_{est}$  derived from the volume of these QSMs, had a mean tree-scale relative error of 3% (table 2). Relative error in up-scaled  $AGB_{est}$  (i.e. the error in the cumulative  $AGB_{est}$  of the four trees) was 1%.

The mean tree-scale relative error in allometric-derived  $AGB_{est}$  was 15%, and the relative error in up-scaled  $AGB_{est}$  was also 15%. Overall then, the lidar methods returned more accurate predictions than allometry (table 2). Precision-wise (random error), the standard deviation of the error in lidar-derived estimates was considerably smaller: 185 kg versus 2523 kg. These estimates were also more true (systematic error), but did tend to be underestimates (mean error:  $-70\ kg$  versus 1398 kg).

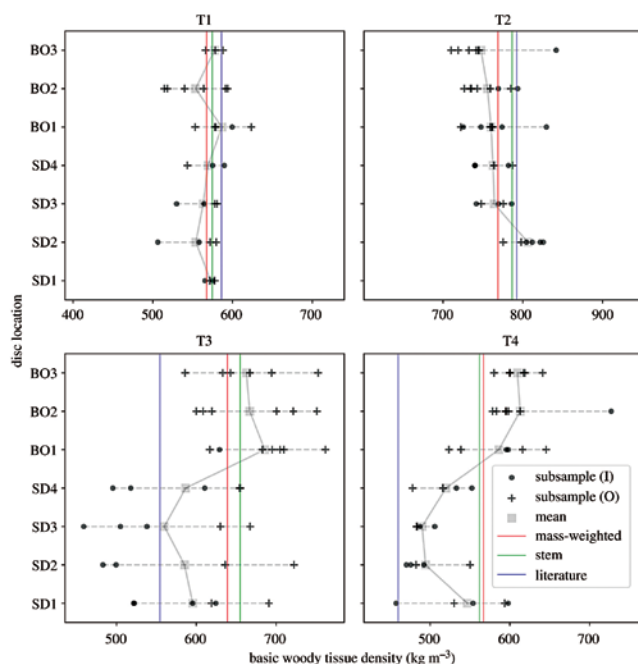


Figure 4. Intra-tree variations in basic woody tissue density with height, for the four harvested trees (T1–T4). Discs were collected from the stem of each tree at 1.3 m above-ground, and at 25%, 50% and 75% along the length of the stem (SD1–SD4, respectively). Discs were also taken from the midpoints of first-, second- and third-order branches (BO1–BO3, respectively). A minimum of 11 discs were collected per tree. These discs were reduced to subsamples using a consistent approach (figure 2), such that any given set of subsamples covered the full length of the major axis of each disc. Each datum represents a measurement of basic woody tissue density on a subsample: crosses represent outer subsamples (i.e. they included periderm, phloem and cambium tissues), and dots represent inner subsamples. The mean density at each disc location is marked by a grey square, and the solid grey interpolation line links these averages throughout each tree. The horizontal dashed grey lines show the range of density values per location, and each plot has an overall range of 350  $kg\ m^{-3}$  for comparative purposes. The vertical lines represent the estimates of above-ground basic woody tissue density derived from the three considered approaches: mass-weighted (red), stem (green) and literature (blue).

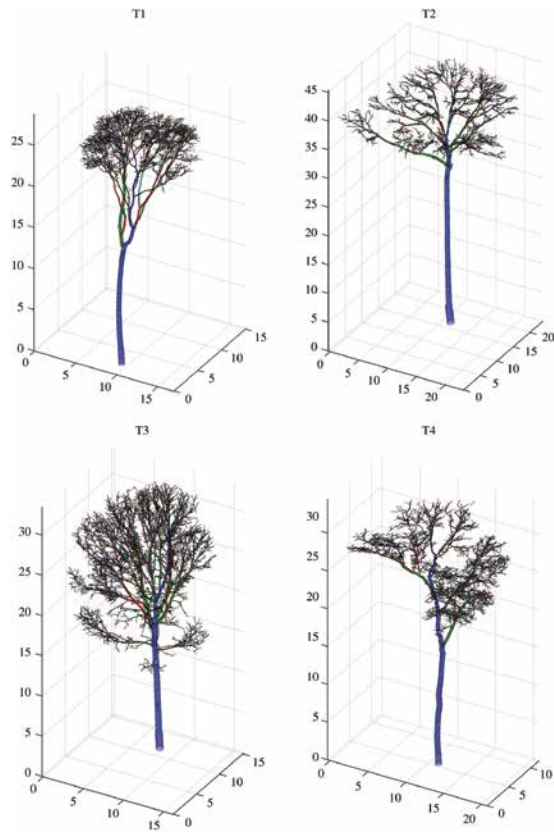


Figure 5. Three-dimensional views of the quantitative structural models representing the four harvested trees. All dimensions in metres. These cylinder models were constructed from the woody point clouds shown in figure 3 using treeqsm [31]. Colours correspond to branching order (i.e. blue, green and red represent stem, first- and second-order branches, respectively).

The lidar methods also accurately estimated the allocation of AGB intra-tree, as illustrated in figure 6. This compares the distributions of AGB between the stem and crown, for both these estimates and the reference measurements. The distributions are similar: 48%, 58%, 38% and 41% of harvest-derived  $AGB_{ref}$  was found in the stems of T1–T4, respectively, while 48%, 62%, 42% and 47% of lidar-derived  $AGB_{est}$  was, respectively, allocated to each stem.

Finally, the approach to estimating above-ground basic woody tissue density was an important determinant of error (figure 7). For the lidar methods, the values derived from direct disc measurements provided estimates with the smallest error:

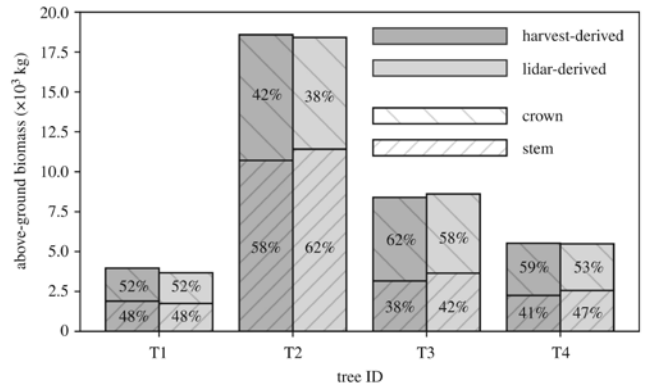
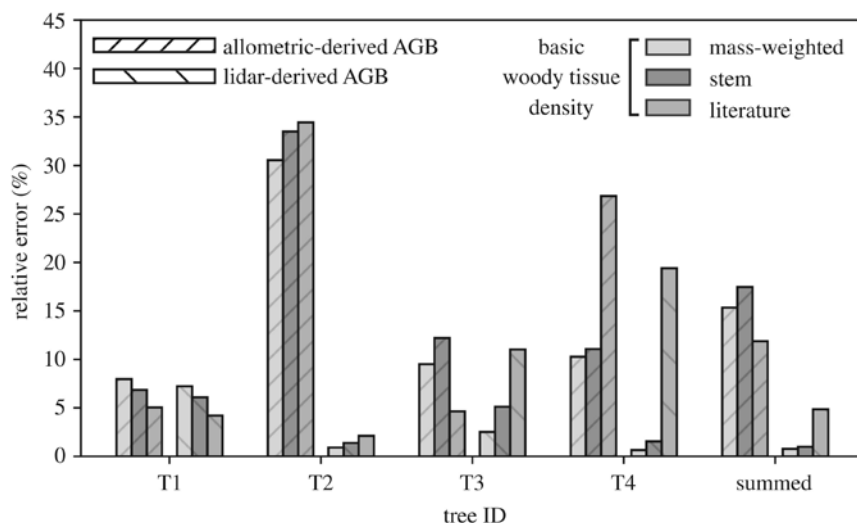


Figure 6. Comparison between the reference harvest-derived measurements of above-ground biomass (AGB), and the lidar-derived estimates. Estimates were calculated using the above-ground green woody volumes provided by the quantitative structural models shown in figure 5, and the corresponding mass-weighted estimates of above-ground woody tissue density. Also shown for both approaches, are the distributions of AGB between the stem and crown.

Table 2. The performance of lidar- and allometric-derived estimates of above-ground biomass ( $AGB_{est}$ ). (Estimates from both approaches were calculated using the mass-weighted estimate of above-ground basic woody tissue density, and compared with the harvest-derived reference values ( $AGB_{ref}$ ). The upper table reports the error in these estimates. Mean relative error is the average of tree-scale relative errors. Summed values refer to the cumulative AGB of the four trees. The lower table quantifies the trueness, precision and accuracy of these estimates.)

ID	$AGB_{ref}$ (kg)	terrestrial lidar			pan-tropical allometry		
		$AGB_{est}$ (kg)	error (kg)	relative error (%)	$AGB_{est}$ (kg)	error (kg)	relative error (%)
T1	3960.1	3673.8	-286.3	7.2	3644.9	-315.2	8.0
T2	18584.2	18414.5	-169.7	0.9	24261.0	5676.8	30.5
T3	8392.6	8604.6	212.0	2.5	9190.9	798.3	9.5
T4	5521.1	5485.1	-36.0	0.7	4953.7	-567.4	10.3
mean	-	-	-	2.8	-	-	14.6
summed	36458.0	36177.9	-280.1	0.8	42050.5	5592.5	15.3
estimation method							
error type	performance characteristic	quantitative metric		terrestrial lidar	pan-tropical allometry		
systematic	trueness	mean error (kg)		-70.0	1398.1		
random	precision	standard deviation of the error (kg)		185.3	2523.2		
total	accuracy	root mean square error (kg)		191.1	2884.7		





**Figure 7.** The impact of different approaches to estimating above-ground basic woody tissue density on the relative error in allometric- and lidar-derived estimates of above-ground biomass (AGBest). Here, the mass-weighted, stem and literature values reported in table 1 were used in the calculation of AGBest. Summed values refer to the cumulative AGB of the four trees.

mean tree-scale relative error in  $AGB_{est}$  using the mass-weighted, stem and literature estimates was 3%, 4% and 9%, respectively. This was less marked for the allometric estimates, with mean tree-scale relative error remaining largely constant across the three approaches (15%, 16% and 18%, respectively).

## 4. Discussion

The destructive measurements provide a rare insight into the considerable variability in large tropical tree structure. The distribution of AGB between the stem and crown of the four trees varied widely, with the crown mass ratio ranging from 0.42 to 0.62 (figure 3). Above-ground basic woody tissue density was estimated (via the mass-weighted approach) to range from 567 to 769  $kg\ m^{-3}$  across the four trees. Density was also observed to vary substantially intra-tree, with both height and radius, and further, these variations were not systematic between trees (figure 4). Less variable were above-ground woody tissue green-to-dry mass and volume ratios: the moisture content of green mass varied from 39 to 42%, and green woody tissues shrank by 10–14% after drying (table 1).

The harvest measurements found  $AGB_{ref}$  of the trees to total 36 458 kg. Non-destructive  $AGB_{est}$  from the lidar- and allometric-derived methods totalled 36 178 kg and 42 051 kg, respectively (table 2). The mean tree-scale relative error was 3% and 15%, respectively. In addition to smaller error, lidar-derived estimates had two further advantages. First, error did not increase with increasing tree size (i.e. stem diameter and tree height), and second, error reduced when up-scaling to the cumulative of the four trees.

### 4.1. Lidar-based methods can accurately estimate above-ground biomass

It was noted in the introduction that error in pan-tropical tree-scale  $AGB_{est}$  from allometry is multiplicative (i.e. error is proportional to tree size), and that it would not be unreasonable to expect uncertainty from random error to remain upwards of 40% at the 1 ha stand-scale. Uncertainty then, in current best estimates of stand-scale AGB, is, in absolute terms, potentially large, and relatively, a function of plot composition. These uncertainties form the current minimum uncertainty in larger-scale AGB estimates (e.g. Amazonia), because such

estimates are themselves invariably reliant upon calibration from forest stands characterized by allometry. The results from this study suggest terrestrial lidar methods have the potential to reduce these uncertainties by more than an order of magnitude, which would enable the production of significantly more accurate estimates of larger-scale carbon stocks.

Overall, lidar-derived  $AGB_{est}$  provided a 15-fold increase in accuracy over allometric counterparts (RMSE difference, table 2). There were two important characteristics that further differentiated these estimates: (i) error in lidar-derived  $AGB_{est}$  did not increase with tree size: tree-scale relative error in the smallest and largest tree was 7% and 1%, respectively (versus 8% and 31%); and (ii) error in lidar-derived  $AGB_{est}$  reduced when up-scaling from the tree-scale, to the cumulative of the four trees: mean tree-scale relative error was 3%, and the relative error in cumulative  $AGB_{est}$  was 1% (versus 15% and 15%). Combined, these results suggest that error in these particular lidar-derived estimates was additive (i.e. errors are not correlated with tree size) and random (i.e. errors are not correlated with one another). If these characteristics, derived from high-quality data collected on a small sample of four trees, were transferable across forest scenes, then error in lidar-derived stand-scale  $AGB_{est}$  would be independent of the size of the trees comprising the stand, and reduce as the number of trees inside the stand increases.

Interestingly, the lidar-derived estimates presented here were also substantially more accurate than those from other studies, where estimates were accompanied by reference harvest data. As discussed in the introduction, two previous experiments have been conducted in tropical forests [35,36], and in both, it was found mean tree-scale relative error in lidar-derived  $AGB_{est}$  exceeded 20% (versus 3% observed here). Because these lidar-derived estimates are generated from explicit three-dimensional models of tree structure, errors arise from two

sources: the estimation of volume, and the estimation of density. Discussed below, we believe recent advances in processing methods have significantly reduced error in estimating volume. However, knowledge gaps remain, particularly in the estimation of density. These knowledge gaps will require filling before lidar-derived estimates are considered both consistently true and precise.

#### 4.1.1. Retrieving above-ground green woody volume from lidar point clouds

A laser scanner estimates the range to targets illuminated by the laser pulse, from timing measurements on the returned radiation. A sequence of methods are required to go from collecting these range estimates, to estimating volumes. Many sources of error exist in these methods, which can be broadly classified into two categories: those arising from data acquisition, and those arising from data processing.

Occlusion is an important source of error in the first category (i.e. tree components obscured by foreground objects). The impacts of occlusion on data quality are driven by multiple factors including the complexity of the scene, increasing distance between sequentially fired pulses with increasing range, instrument characteristics (e.g. beam divergence), and the user-defined sampling protocol. Other sources of error in the first category include the instrument itself (e.g. ranging accuracy), environmental impacts including wind and rain, and the inability to collect data from inside the tree (e.g. information on internal cavities). Sources of error in the second category are specific to the particular processing chain, but here, would include those arising from: (i) the registration of individual scans onto a common coordinate system, (ii) the segmentation of individual trees from the larger-area point cloud, (iii) the classification of points as returns from wood or leaf surfaces, (iv) the manual removal of points from buttresses, and (v) the approach to constructing QSMs (e.g. cylinders were used here to model woody structure).

It is impossible here to attribute the observed differences in  $AGB_{est}$  and  $AGB_{ref}$  to any of these sources. Indeed, attributing error to either top-level error source (i.e. the estimate of volume or density) is difficult. That is, we cannot explicitly explain the error because we do not have control over these individual sources, and because these errors are often related in complex ways (e.g. occlusion will affect the goodness of a cylinder fit). However, we have demonstrated that given occlusion minimized high-quality terrestrial lidar data, it can be expected that current open-source processing tools are capable of estimating large tropical tree AGB to within a few percent of reference measurements, despite these potential sources of error in volume estimation.

We think the recent development of wood-leaf separation algorithms has been an important step forward in enabling this [27,30]. This is illustrated in the electronic supplementary material, appendix B, where it is demonstrated that when returns from leafy surfaces are allowed to interfere in woody reconstruction,  $AGB_{est}$  is substantially overestimated, with the relative error in cumulative  $AGB_{est}$  increasing to upwards of 40%. This is further corroborated by figure 6, which demonstrates that the lidar methods were able to accurately resolve the allocation of AGB between the stem and crown of each tree. That is,  $AGB_{est}$  did not accidentally agree with  $AGB_{ref}$  because of underestimation in the stem and overestimation in the crown, but because of close agreement in both pools. We recommend then, that for the particular processing methods used here, removing leaf returns from point clouds is a critical step in accurately retrieving  $AGB_{est}$  from occlusion minimized high-quality terrestrial lidar data collected in evergreen forests, or from so-called ‘leaf-on’ point clouds.

#### 4.1.2. The more tricky issue of density

The other top-level source of error in lidar-derived  $AGB_{est}$  is in the estimation of density. As described in the introduction, if we were to assume an estimate of a

tree’s above-ground green woody volume is error free, then to convert this into an unbiased estimate of AGB (assuming the contribution by leaf material to AGB is negligible), the above-ground basic woody tissue density is required. We have intentionally used this specific term throughout the paper because the value is required to: (i) convert a green volume into a dry mass, (ii) account for the density of each woody tissue filling the volume, by the relative abundance of each tissue, and (iii) account for the variations in the density of these tissues throughout the tree.

However, this variable is largely immeasurable because it requires above-ground woody weighing and water displacement. Here, the mass-weighted approach most closely resembled its measurement (i.e. weighting the mean basic woody tissue density from the disc subsamples in each pool, by the green mass in each pool). This mass-weighted approach illustrates how the more indirect methods for estimating above-ground basic woody tissue density introduce error into lidar-derived  $AGB_{est}$  (figure 7). For example, the approach intended to mimic measurements on cores acquired from increment boring (i.e. stem: calculated from the mean woody tissue density of the two outer subsamples taken from the stem disc collected at 1.3 m above-ground), increased mean tree-scale relative error from 3%, to 4%. Similarly, when we used values from the Global Wood Density Database [39], error increased to 9%. The point then, is that whenever non-destructive lidar-derived AGB estimates are required, the only practicable approaches to estimating above-ground basic woody tissue density are to use values obtained from increment boring or from the literature. The question is, are there any reliable methods to account for error arising from the inability to directly measure above-ground basic woody tissue density?

One approach is convert values obtained from either of these methods via some correction factor. Sagang *et al.* [33] and Momo *et al.* [43] have recently explored this approach for tropical forests in

Central Africa. In these studies, data from destructive measurements ( $n = 130$  and  $822$  trees, respectively) were used to construct models to convert literature- or increment boring-based values to more closely mirror above-ground basic woody tissue density. Momo et al. [43] also captured terrestrial lidar data for a subset of these harvested trees ( $n = 58$ ), and demonstrated error in lidar-derived  $AGB_{est}$  reduced when these corrective models were applied.

It would be unreasonable to apply the published corrective models to the data collected here, given the substantial variations observed within and between tropical regions [19]. It is however perhaps worth noting the top-level consequence had they been applied: our stem- and literature-derived estimates of above-ground basic woody tissue density would have been pushed downwards by approximately 21% and 36%, respectively, and therefore significantly below the mass-weighted estimates (figure 4). Here then, this behaviour would have greatly increased tree-scale relative error in lidar-derived  $AGB_{est}$  for all four trees.

This is not to suggest such models are necessarily inappropriate at a larger-scale, (e.g. an equivalent model constructed from Amazonia data could be directionally correct), but at the out-of-sample tree- or stand-scale, it is impossible to know whether their application would have a beneficial or detrimental impact on error in  $AGB_{est}$ . Another important consideration for these models in the context of Amazonia is the hyperdominance of certain species [44]. That is, it is not necessarily sufficient for these models to accurately correct for the majority of species in the Amazon, if a large portion of Amazon-scale  $AGB$  is stored in a relatively small number of key species.

We would suggest then, there is currently no simple approach to account for error in lidar-derived  $AGB_{est}$  arising from the inability to measure above-ground basic woody tissue density. In the longer-term, hopefully new non-destructive estimation methods will be pioneered,

with interesting research ongoing using genomics [45]. However, in the meantime, our recommendation from the analysis of the data collected here, is that when viable, density estimates acquired from direct measurements on the stems of trees are probably superior to those taken from the literature (mean tree-scale relative error of 4% and 9%, respectively).

#### 4.1.3. Improving uncertainty quantification

It is important to be able to assign meaningful uncertainty intervals to any non-destructive estimate of  $AGB$ , whether allometric- or lidar-derived, and whether at tree- or stand-scale. That is, when such methods are applied to a tree or stand where destructive validation measurements are unavailable, what is the uncertainty in subsequent estimates?

As discussed above, our analysis of the data collected from this sample of four large tropical trees identified: (i) error in lidar-derived  $AGB_{est}$  did not increase with increasing tree size, and (ii) error in  $AGB_{est}$  reduced when up-scaling from tree-scale, to the cumulative of the four trees. It would therefore be reasonable to suggest the following hypothesis: error in terrestrial lidar-derived tree-scale  $AGB_{est}$  is additive and random. If this were provisionally confirmed, then to assign meaningful uncertainty intervals to out-of-sample tree- and stand-scale  $AGB_{est}$  would only require a robust understanding of the variance in the error. To test this hypothesis, further destructive validation data similar to those collected here are required. In particular, it would be necessary to have some confidence that these new data attempted to capture the bounds of variability in above-ground volume and woody tissue density. That is, these data would ideally be collected from a range of different forest types, species, size classes and crown forms.

If such data were to be collected, then we think priority should be placed on two further considerations. First, on understanding the implications of lidar data quality on error. That is, how scene

complexity, instrument and sampling patterns change random error variance and/or introduce systematic error. We note that in this experiment, the lidar data were collected after neighbouring vegetation surrounding each tree was removed, meaning data quality is probably higher than equivalent data collected in a non-destructive setting.

Second, the reference measurements should be collected from direct measurement of green mass (i.e. not indirectly estimated via geometry measurements), to ensure reference values are as close to true as possible. The measurements collected in this experiment illustrate how important this point is: during the harvest, each stem was cut into manageable sections, on which length and diameter measurements were made, permitting estimation of geometry-derived (Smalian's formula) green stem mass via the mass-weighted estimate of above-ground green woody tissue density. A percentage error of -1%, 7%, 11% and 11% was observed when these estimates were compared with direct weighing measurements for T1-T4, respectively. These are large errors, and their presence in reference data would lead to spurious interpretations of the error in lidar- or allometric-derived  $AGB_{est}$ .

#### 4.2. Capturing the variation in tropical tree structure

We finish with a brief comment on the potential applications of the terrestrial lidar data beyond  $AGB$  estimation. The harvest measurements identified that for three out of the four trees, the majority of  $AGB$  was most often stored in the crown, with the crown mass ratio ranging from 0.42 to 0.62 (figure 3). Both this result, and the variation itself, is consistent with previously published data for large tropical trees in forests similar to our site [13], and also somewhat in agreement with data collected from across the tropics [12,46]. However here, the lidar point clouds (figure 3), which provide a unique perspective on tree structure, can begin to offer some insights into this variability. That is, these clouds permit

quantification of crown form: the crown-to-tree height ratio was 0.55, 0.40, 0.54 and 0.56 for T1–T4, respectively, and the crown aspect ratio (diameter of the major axis over crown height) was 1.15, 1.63, 1.18 and 1.44, respectively. A relatively shallow, albeit wider crown then, provides a structural reason for T2 being the only sampled tree with the majority of AGB in the stem (it is perhaps also worth noting T2 was the only tree whose crown was found in the emergent layer of the stand). The underlying causal explanation for the form of a tree's crown is the result of an intricate balancing act between multiple genetic and ecosystem factors [47]. The QSMs then (figure 5), which explicitly describe three-dimensional tree architecture through to high order branching, provide a novel platform for ecologists to explore these interactions between tree architecture and ecological function [48,49].

## 5. Conclusion

In conclusion, we harvested four large tropical rainforest trees in an intact old-growth forest stand in East Amazonia, and directly weighed their above-ground green mass. We also collected detailed moisture content and woody tissue density measurements throughout each tree. We first presented some rare ecological insights provided by these data, including on the considerable structural variability of these trees, in terms of both the distribution of mass between stem and crown, and the substantial intra-tree variations in woody tissue density. We then assessed the performance of new terrestrial lidar-based methods for non-destructive estimation of the AGB of these trees, using high-quality three-dimensional measurements collected pre-harvest. This study presented, to our knowledge, the first validation of such estimates from tropical forests using reference data that were derived entirely from direct measurement. We found these estimates were accurate, and a 15-fold improvement over counterparts derived from classical allometry. The results also provided evidence to suggest error in

these estimates was random and additive. If this performance were transferable across forest scenes, then these terrestrial lidar methods would enable significantly more accurate estimates of larger-scale carbon stocks. We suggested that a more robust understanding of the error in lidar-derived AGB estimates can only be achieved through the collection of further validation data.

## Data accessibility

Data from the destructive measurements are archived at <https://doi.org/10.5281/zenodo.4056899>. Data from the terrestrial lidar measurements are archived at <https://doi.org/10.5281/zenodo.4056903>. TreeSEG is available at <https://github.com/apburt/treeseg>, and the version used in this paper, v. 0.2.0, is archived at <https://doi.org/10.5281/zenodo.3739213>. TLSeparation is available at <https://github.com/TLSeparation>, and the version used in this paper, v. 1.2.1.5, is archived at <https://doi.org/10.5281/zenodo.1147706>. TreeQSM is available at <https://github.com/InverseTampere/TreeQSM>, and the version used in this paper, v. 2.3.2, is archived at <https://doi.org/10.5281/zenodo.3560555>. optQSM is available at <https://github.com/apburt/optqsm>, and the version used in this paper, v. 0.1.0, is archived at <https://doi.org/10.5281/zenodo.3911269>.

## Authors' contributions

All authors designed the methods, and collected and analysed the data. A.B. wrote the manuscript, with contributions from all authors.

## Competing interests

We declare we have no competing interests.

## Funding

A.B. and M.D. acknowledge funding from Natural Environment Research

Council (NERC) grant no. NE/N00373X/1 and European Research Council grant no. 757526. A.C.L.d.C. acknowledges funding from Conselho Nacional de Desenvolvimento Científico e Tecnológico (CNPq) grant no. 457914/2013-0/MCTI/CNPq/FNDCT/LBA/ESECAFLOR. P.M. acknowledges funding from NERC grant no. NE/N006852/1. L.R. acknowledges funding from NERC independent fellowship grant no. NE/N014022/1. M.D. also acknowledges funding from NERC National Centre for Earth Observation (NCEO, NE/R016518/1).

## Acknowledgements

We thank ICMBio (Instituto Chico Mendes de Conservação da Biodiversidade) for providing the land to conduct this experiment. We thank the Museu Paraense Emílio Goeldi for providing logistical support. We gratefully acknowledge Cleidemar Araujo de Souza, Filomeno Martins do Amaral Filho, Josenildo Costa Amaral, Juscelino Costa Amaral, Moises Moraes Alves and Raimundo de Souza Brasão Júnior for collecting the harvest data.

## References

1. Baccini A *et al.* 2012 Estimated carbon dioxide emissions from tropical deforestation improved by carbon-density maps. *Nat. Clim. Change* 2, 182–185. (doi:10.1038/nclimate1354)
2. Mitchard ETA *et al.* 2014 Markedly divergent estimates of Amazon forest carbon density from ground plots and satellites. *Glob. Ecol. Biogeogr.* 23, 935–946. (doi:10.1111/geb.12168)
3. Saatchi SS *et al.* 2011 Benchmark map of forest carbon stocks in tropical regions across three continents. *Proc. Natl Acad. Sci. USA* 108, 9899–9904. (doi:10.1073/pnas.1019576108)


4. Hubau W *et al.* 2020 Asynchronous carbon sink saturation in African and Amazonian tropical forests. *Nature* 579,80–87. (doi:10.1038/s41586-020-2035-0)
5. Avitabile V *et al.* 2016 An integrated pan-tropical biomass map using multiple reference datasets. *Glob. Change Biol.* 22, 1406–1420. (doi:10.1111/gcb.13139)
6. Malhi Y *et al.* 2006 The regional variation of aboveground live biomass in old-growth Amazonian forests. *Glob. Change Biol.* 12, 1107–1138. (doi:10.1111/j.1365-2486.2006.01120.x)
7. Martin AR, Doraisami M, Thomas SC. 2018 Global patterns in wood carbon concentration across the world's trees and forests. *Nat. Geosci.* 11, 915–920. (doi:10.1038/s41561-018-0246-x)
8. Nogueira EM, Fearnside PM, Nelson BW, Barbosa RI, Keizer EWH. 2008 Estimates of forest biomass in the Brazilian Amazon: new allometric equations and adjustments to biomass from wood-volume inventories. *For. Ecol. Manage.* 256, 1853–1867. (doi:10.1016/j.foreco.2008.07.022)
9. Brown IF, Martinelli LA, Thomas WW, Moreira MZ, Cid Ferreira CA, Victoria RA. 1995 Uncertainty in the biomass of Amazonian forests: an example from Rondônia, Brazil. *Forest Ecol. Manage.* 75, 175–189. (doi:10.1016/0378-1127(94)03512-U)
10. Chambers JQ, Ribeiro RJ, Higuchi N. 2001 Tree damage, allometric relationships, and above-ground net primary production in central Amazon forest. *Forest Ecol. Manage.* 152, 73–84. (doi:10.1016/S0378-1127(00)00591-0)
11. Chave J *et al.* 2014 Improved allometric models to estimate the aboveground biomass of tropical trees. *Glob. Change Biol.* 20, 3177–3190. (doi:10.1111/gcb.12629)
12. Goodman RC, Phillips OL, Baker TR. 2014 The importance of crown dimensions to improve tropical tree biomass estimates. *Ecol. Appl.* 24, 680–698. (doi:10.1890/13-0070.1)
13. Maia Araújo T, Higuchi N, Andrade de Carvalho Júnior J. 1999 Comparison of formulae for biomass content determination in a tropical rain forest site in the state of Pará, Brazil. *For. Ecol. Manage.* 117,43–52. (doi:10.1016/S0378-1127(98)00470-8)
14. Saldarriaga JG, West DC, Tharp ML, Uhl C. 1988 Long-term chronosequence of forest succession in the upper Rio Negro of Colombia and Venezuela. *J. Ecol.* 76, 938–958. (doi:10.2307/2260625)
15. Brown S. 1997 *Estimating biomass and biomass change of tropical forests*. Rome, Italy: FAO -Food and Agriculture Organization of the United Nations.
16. Slik JWF *et al.* 2015 An estimate of the number of tropical tree species. *Proc. Natl Acad. Sci. USA* 112, 7472–7477. (doi:10.1073/pnas.1423147112)
17. Baker TR *et al.* 2004 Variation in wood density determines spatial patterns in Amazonian forest biomass. *Glob. Change Biol.* 10, 545–562. (doi:10.1111/j.1365-2486.2004.00751.x)
18. Feldpausch TR *et al.* 2012 Tree height integrated into pantropical forest biomass estimates. *Biogeosciences* 9, 3381–3403. (doi:10.5194/bg-9-3381-2012)
19. Phillips OL, Sullivan MJP, Baker TR, Monteagudo Mendoza A, Vargas PN, Vásquez R. 2019 Species matter: wood density influences tropical forest biomass at multiple scales. *Surv. Geophys.* 40, 913–935. (doi:10.1007/s10712-019-09540-0)
20. Kerkhoff AJ, Enquist BJ. 2009 Multiplicative by nature: why logarithmic transformation is necessary in allometry. *J. Theor. Biol.* 257, 519–521. (doi:10.1016/j.jtbi.2008.12.026)
21. Molto Q, Rossi V, Blanc L. 2013 Error propagation in biomass estimation in tropical forests. *Methods Ecol. Evol.* 4, 175–183. (doi:10.1111/j.2041-210x.2012.00266.x)
22. Picard N, Boyemba Bosela F, Rossi V. 2015 Reducing the error in biomass estimates strongly depends on model selection. *Ann. Forest Sci.* 72, 811–823. (doi:10.1007/s13595-014-0434-9)
23. Burt A, Calders K, Cuni-Sanchez A, Gómez-Dans J, Lewis P, Lewis SL, Malhi Y, Phillips OL, Disney M. 2020 Assessment of bias in pan-tropical biomass predictions. *Front. Forests Glob. Change* 3, 12. (doi:10.3389/ffgc.2020.00012)
24. Clark DB, Kellner JR. 2012 Tropical forest biomass estimation and the fallacy of misplaced concreteness. *J. Veg. Sci.* 23, 1191–1196. (doi:10.1111/j.1654-1103.2012.01471.x)
25. Danson FM, Disney MI, Gaulton R, Schaaf C, Strahler A. 2018 The terrestrial laser scanning revolution in forest ecology. *Interface Focus* 8, 20180001. (doi:10.1098/rsfs.2018.0001)
26. Wilkes P, Lau A, Disney M, Calders K, Burt A, Gonzalez de Tanago J, Bartholomeus H, Brede B, Herold M. 2017 Data acquisition considerations for terrestrial laser scanning of forest plots. *Remote Sens. Environ.* 196, 140–153. (doi:10.1016/j.rse.2017.04.030)
27. Boni Vicari M, Disney M, Wilkes P, Burt A, Calders K, Woodgate W. 2019 Leaf and wood classification framework for terrestrial lidar point clouds. *Methods Ecol. Evol.* 10, 680–694. (doi:10.1111/2041-210X.13144)

28. Burt A, Disney M, Calders K. 2019 Extracting individual trees from lidar point clouds using *treeseg*. *Methods Ecol. Evol.* 10, 438–445. (doi:10.1111/2041-210x.13121)
29. Hackenberg J, Spiecker H, Calders K, Disney M, Raumonon P. 2015 Simpletree - an efficient open source tool to build tree models from TLS clouds. *Forests* 6, 4245–4294. (doi:10.3390/f6114245)
30. Krishna Moorthy SM, Calders K, Boni Vicari M, Verbeeck H. 2020 Improved supervised learning-based approach for leaf and wood classification from lidar point clouds of forests. *IEEE Trans. Geosci. Remote Sens.* 58, 3057–3070. (doi:10.1109/TGRS.2019.2947198)
31. Raumonon P, Kaasalainen M, Åkerblom M, Kaasalainen S, Kaartinen H, Vastaranta M, Holopainen M, Disney M, Lewis P. 2013 Fast automatic precision tree models from terrestrial laser scanner data. *Remote Sens.* 5, 491–520. (doi:10.3390/rs5020491)
32. Plourde BT, Boukili VK, Chazdon RL. 2015 Radial changes in wood specific gravity of tropical trees: inter- and intraspecific variation during secondary succession. *Funct. Ecol.* 29, 111–120. (doi:10.1111/1365-2435.12305)
33. Sagang LBT *et al.* 2018 Using volume-weighted average wood specific gravity of trees reduces bias in aboveground biomass predictions from forest volume data. *For. Ecol. Manage.* 424, 519–528. (doi:10.1016/j.foreco.2018.04.054)
34. Calders K *et al.* 2015 Nondestructive estimates of above-ground biomass using terrestrial laser scanning. *Methods Ecol. Evol.* 6, 198–208. (doi:10.1111/2041-210X.12301)
35. Momo ST *et al.* 2018 Using terrestrial laser scanning data to estimate large tropical trees biomass and calibrate allometric models: a comparison with traditional destructive approach. *Methods Ecol. Evol.* 9, 905–916. (doi:10.1111/2041-210X.12933)
36. Gonzalez de Tanago J *et al.* 2018 Estimation of above-ground biomass of large tropical trees with terrestrial lidar. *Methods Ecol. Evol.* 9, 223–234. (doi:10.1111/2041-210X.12904)
37. Meir P, Mencuccini M, Binks O, da Costa AL, Ferreira L, Rowland L. 2018 Short-term effects of drought on tropical forest do not fully predict impacts of repeated or long-term drought: gas exchange versus growth. *Phil. Trans. R. Soc. B* 373, 20170311. (doi:10.1098/rstb.2017.0311)
38. Rowland L *et al.* 2015 Death from drought in tropical forests is triggered by hydraulics not carbon starvation. *Nature* 528, 119–122. (doi:10.1038/nature15539)
39. Chave J, Coomes D, Jansen S, Lewis SL, Swenson NG, Zanne AE. 2009 Towards a worldwide wood economics spectrum. *Ecol. Lett.* 12, 351–366. (doi:10.1111/j.1461-0248.2009.01285.x)
40. RIEGL Laser Measurement Systems GmbH 2018, Riscan pro. See <http://www.riegl.com>.
41. *CloudCompare* 2019. See <https://cloudcompare.org/>.
42. Menditto A, Patriarca M, Magnusson B. 2007 Understanding the meaning of accuracy, trueness and precision. *Accredit. Qual. Assur.* 12, 45–47. (doi:10.1007/s00769-006-0191-z)
43. Momo ST *et al.* 2020 Leveraging signatures of plant functional strategies in wood density profiles of African trees to correct mass estimations from terrestrial laser data. *Sci. Rep.* 10, 2001. (doi:10.1038/s41598-020-58733-w)
44. ter Steege H *et al.* 2013 Hyperdominance in the Amazonian tree flora. *Science* 342, 1243092. (doi:10.1126/science.1243092)
45. Baisson J *et al.* 2019 Genome-wide association study identified novel candidate loci affecting wood formation in norway spruce. *Plant J.* 100, 83–100. (doi:10.1111/tj.14429)
46. Ploton P *et al.* 2016 Closing a gap in tropical forest biomass estimation: taking crown mass variation into account in pantropical allometries. *Biogeosciences* 13, 1571–1585. (doi:10.5194/bg-13-1571-2016)
47. Verbeeck H, Bauters M, Jackson T, Shenkin A, Disney M, Calders K. 2019 Time for a plant structural economics spectrum. *Front. For. Glob. Change* 2, 43. (doi:10.3389/ffgc.2019.00043)
48. Disney M. 2019 Terrestrial lidar: a three-dimensional revolution in how we look at trees. *New Phytol.* 222, 1736–1741. (doi:10.1111/nph.15517)
49. Meir P, Shenkin A, Disney M, Rowland L, Malhi Y, Herold M, da Costa ACL. 2017 *Plant structure-function relationships and woody tissue respiration: upscaling to forests from laser-derived measurements*. pp. 89–105. Cham, Switzerland: Springer.

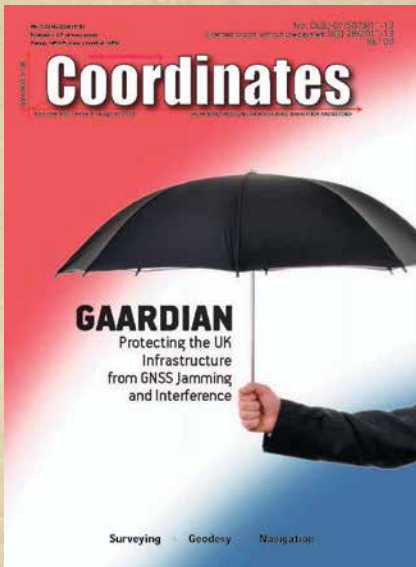
## Footnotes

Electronic supplementary material is available online at <https://doi.org/10.6084/m9.figshare.c.5289071>.

© 2021 The Authors.

Published by the Royal Society under the terms of the Creative Commons Attribution License <http://creativecommons.org/licenses/by/4.0/>, which permits unrestricted use, provided the original author and source are credited. 

# In Coordinates



[mycoordinates.org/vol-8-issue-8-August-2012](http://mycoordinates.org/vol-8-issue-8-August-2012)

## The Jamaica VRS and Cadastral Surveying

**Glendon G Newsome, Gregory Peake and Romaine Douglas**  
University of Technology, Jamaica

Unique and precise coordinates will be provided for each point that is coordinated with this system as it will be configured to function in the JAD2001 datum

## Geoid modelling

**K F Aleem**  
Department of Geomatics Engineering  
Technology, Yanbu Industrial College,  
Yanbu Industrial City, Saudi Arabia

In this study, levelled heights were established and the benchmarks were coordinated and collocated with both GPS and geodetic levelling in the Port Harcourt Metropolis. Optimal predictive geoid models 'Satlevel' for deriving orthometric height from ellipsoidal heights on the WGS 84 reference ellipsoid were developed

# 10 years before...

## GAARDIAN: A system to detect GNSS jamming and Interference

**Andy G Proctor**  
Divisional Manager GNSS  
Applications and Solutions,  
Chronos Technology Ltd., UK

**Charles W T Curry**  
Managing Director, Chronos  
Technology Ltd., UK

**Jenna Tong**  
Postdoctoral Researcher, Electronic  
and Electrical Engineering  
Department, University of Bath, UK

**Robert Watson**  
Senior Lecturer, Electronic  
and Electrical Engineering  
Department, University of Bath

**Mark Greaves**  
Geodetic Analysts  
Ordnance Survey

**Paul Cruddace**  
Geodesy and Positioning  
Manager Ordnance Survey

The GAARDIAN program completed in 2011. This article gives an overview of the resulting capability to detect GNSS interference and jamming. It also provides details about a specific recent detection event that demonstrated the capability of the system and that, by involving UK Law enforcement agencies, proved the system can be operationally effective

## INS-GPS-GLONASS navigation fusion scheme for high dynamics guided projectiles

**G Sathesh Reddy and Manjit Kumar**  
Research Center Imarat, Defence Research and Development  
Organisation (DRDO), Hyderabad, India

In degraded signal environments the accuracy and availability of the GPS are affected for Kinematic applications. To address this issue, combined GPS- GLONASS systems are studied for various Low and High Dynamics applications using tightly coupled GG aided INS solutions to overcome the problem of using single constellation when we desire to achieve reliable high terminal accuracy for Inertial Guided Vehicles

## eHarta tryst with Romania

**Codrina Maria Ilie**  
Board Member [geo-spatial.org](http://geo-spatial.org)

eHarta is a collection of thousands of georeferenced historical maps, published and documented with the help of the community. It is a collaborative initiative to digitally preserve and freely share old cartographic documents

---

## Rwanda joins ADB supported remote data collection initiative

Rwanda has embraced the Remote Appraisal, Supervision, Monitoring and Evaluation (RASME) initiative, a tool that enhances project-related data collection in remote areas. It is the first East African country to do so and the seventh overall in the continent.

The initiative is a partnership of the African Development Bank's IT Department (CHIS), the World Bank's Geo-Enabling initiative for Monitoring and Supervision, and KoBoToolbox Foundation, a non-governmental organization affiliated with the Harvard Humanitarian Initiative.

RASME enables Bank staff, including task and sector managers, country and regional program officers, and government officials, to compile project information directly from the field, using a smartphone, tablet or laptop, drones and satellites. The data is gathered in various formats, including text, video, graphics and even survey responses. [www.afdb.org](http://www.afdb.org)

---

## Strong progress being made on the UK's Geospatial Strategy

Rolling out the National Underground Assets Register, piloting public sector access to commercial satellite data and publishing expert guidance on investing in location data are among the key priorities for the Geospatial Commission over the next year.

The Geospatial Commission has published on 22 June its plan for 2022/23, which sets out priorities for the coming year and reflects on the growing use of location data as a strategic national asset to support levelling up, help meet net zero targets and drive science and technology innovation.

The Geospatial Commission's priorities for the coming year are:

- Continuing to rollout the National Underground Assets Register (NUAR) to build a shared, national underground utilities data asset to improve safe

digging and UK-wide infrastructure delivery, realizing at least £345 million of economic value each year

- Piloting public sector access to commercial satellite data, to better understand whether collective access will help overcome barriers to the wider public sector adoption of Earth Observation data
- Publishing guidance about how to make an effective case for investing in location data, ensuring that its full value is well understood, assessed, and articulated.

[www.gov.uk](http://www.gov.uk)

---

## 1Spatial improves portal to simplify data handling

1Spatial are improving their data submission portal, 1Data Gateway, to further simplify and minimize data handling within their solutions.

Following one of 1Spatial's key Location Master Data Management principles – Simplify and Minimise Data Handling – many enhancements to 1Data Gateway 2.6 focus on reducing processing time. This latest release has seen the 1Spatial Team adding schema management enhancements to make complex data submissions even simpler to manage, accept and process. <https://1spatial.com/au/>

---

## Oil India selects Juniper Networks

Juniper Networks have been selected by Oil India Limited for upgrades to its data center and campus networks to support the company's sustainability goals and digital transformation journey that will contribute to India's vision of energy independence.

Juniper's QFX5120 Series Switches were deployed in the data centers at Oil India's headquarters in Duliajan, Assam, while the combination of QFX5120 and QFX5110 Switches serve as a resilient campus core. Oil India also selected the EX4300 Series Switches for its campus distribution layer and adopted a Spine-Leaf architecture with EVPN-VXLAN for the campus core.

---

## BASEMAP announces £3.2M PSGA contract with OS

Basemap has signed a £3.2 Million contract with Ordnance Survey (OS) to provide data for The Public Sector Geospatial Agreement.

PSGA is a contract between the Geospatial Commission, on behalf of the public sector in England, Wales, Scotland, and Ordnance Survey and it provides the route for public sector members to access, use and share location data. Basemap's Speed Limit data is the most detailed dataset for roads in Great Britain and its Average Speed data offers 100% coverage across all of Great Britain's roads. [www.basemap.com](http://www.basemap.com)

---

## NavVis & Magic Leap partner to enable enterprise-ready 3D mapping

NavVis and Magic Leap have announced a strategic partnership to deliver large-scale Augmented Reality (AR) applications in complex enterprise environments.

Combining Magic Leap's advanced spatial computing platform with NavVis's mobile mapping systems and spatial data platform, the two companies aim to enhance the use of AR applications across key industries, including automotive and manufacturing, with comprehensive, photorealistic, and accurate 3D digital twin data. [www.magicleap.com](http://www.magicleap.com)

---

## ICE launches the ESG Geo-Analyzer

Intercontinental Exchange, Inc has launched the ICE ESG Geo-Analyzer, which leverages ICE's geospatial data modelling to provide climate risk and social impact data and analytics for properties and communities throughout the U.S.

The ICE ESG Geo-Analyzer is an on-demand platform that takes user-provided location data including street address, latitude / longitude, or zip code to analyze the climate risk and social impact characteristics surrounding any location or portfolio of properties, within



the contiguous U.S. It can be used to analyze commercial and residential properties, whole loan portfolios and real estate holdings, and the asset-backed securities or business and corporate operations tied to those locations. The ICE ESG Geo-Analyzer will cover additional geographies globally in 2023. [www.theice.com](http://www.theice.com)

---

### SAP customers control their Data in the Cloud

Thales announced a new cloud data protection solution that will protect SAP customers' sensitive data in SAP applications in public cloud environments. Together, the two companies are offering new capabilities that enable security teams to own and centralize the control of their encryption keys across public clouds while helping meet compliance and regulatory requirements.

---

### Envitia Partnership with Italian geospatial company GeoSolutions

Envitia has partnered with Italian Geospatial Company GeoSolutions to provide exclusive enterprise-level deployment, integration and support for its open-source tools in the UK. The partnership will see Envitia support its suite of products in the UK, including GeoServer, Mapstore, and Geonode. These tools provide critical functionality for companies to share, process, and edit geospatial data, manage, and securely share maps, and create, save, browse and share maps using content from sources. [envitia.com](http://envitia.com)

---

### Siemens partnership with Esri

Siemens Smart Infrastructure has partnered with Esri to expand its ecosystem of partners for its grid software business. The partnership hopes to enhance capabilities for the planning, operations and maintenance of power networks at grid operators by combining Esri's mapping and spatial analytics software and Siemens' electrical topology expertise. ▽

---

### Consortium to develop future European land combat capabilities

Already member of the Consortium and part of the FAMOUS effort, Arqus has announced that it has been selected as a part of FAMOUS2, alongside coordinator Patria from Finland, fellow French major Defense company and partner Nexter, as well as 15 other leading companies from Finland, Austria, Germany, Spain, Greece, Belgium, Norway, Latvia and Denmark.

The project is supported by nine countries including France and will be funded by the EU just short of 95 million euros. It is a major step forward for European defense industrial cooperation, as well as for Arqus which will take part in a most ambitious and exciting land defense program which should help shape the future of European land defense.

The FAMOUS2 project aims at developing innovative technological building blocks for the next generation armored platforms and upgrades existing platforms, such as future all-terrain vehicle (ATV), light armored vehicle (LAV) and Main Battle Tank (MBT). It is building on the ongoing EDIDP 2020 FAMOUS project, thus following-up the research on vehicles and systems concepts during this precursor project. The FAMOUS2 project should start by 2023 and end by 2026 and will focus on vehicle architecture, which will be followed by the designing, building and testing of prototypes developed in that framework.

Arqus will play a major role within FAMOUS2, especially in vehicle architecture, mobility and power. Through this project, Arqus will participate in enhancing the capabilities, innovation and cooperation levels among European Defense key players. [www.arqus-defense.com](http://www.arqus-defense.com)

---

### Russia to deploy GLONASS station in Venezuela

Russia will mark the GLONASS ground station on the territory of Venezuela. As part of the implementation of the provisions of the agreement between the government of the Russian Federation

and the government of the Bolivarian Republic of Venezuela on cooperation in the exploration and use of outer space for peaceful purposes, signed on March 30, 2021 and ratified on June 11, 2022, the state corporation Roskosmos plans to deploy an uninterrupted measuring station (LIS) of the GLONASS system in Venezuela. It is indicated that the measuring stations are designed to provide high-precision navigation for consumers using Precise Point Positioning technology. <https://thesaxton.org>

---

### SBG Inertial Navigation System

The Quanta Micro GNSS-aided inertial navigation system (INS) offers a high level of navigation performance despite its low size, weight, power and cost (SWAP-C). It brings direct georeferencing to UAV and land-based surveying. It leverages a survey-grade inertial measurement unit (IMU) for optimal heading performance in single-antenna applications, and high immunity to vibrating environments. An optional secondary antenna enables fast heading initialization in low dynamic applications. [sbg-systems.com](http://sbg-systems.com)

---

### Russian military launches GLONASS-K navigation satellite from Plesetsk

The Russian Aerospace Forces (VKS), itself a division of the Armed Forces of the Russian Federation, continued to build on their 2022 campaign with the successful launch of a GLONASS-K navigation satellite on a Soyuz rocket. The launch, which took place from Site 43/4 at the Plesetsk Cosmodrome in northwestern Russia, occurred at approximately 09:18 UTC on Thursday, July 7. This marked the ninth launch of the year so far for the Russian Federation, with all of them utilizing various adaptations of the Soyuz launch vehicle. Thursday's flight also marked the fifth launch of 2022 for the Russian military. The GLONASS-K satellites stand as substantial improvements over the previous-generation GLONASS-M constellation, having a longer lifetime and better signals accuracy. [www.nasaspacelflight.com](http://www.nasaspacelflight.com) ▽

---

## Enhancing Living Atlas of the world

Maxar Technologies has announced that Esri, will enhance the World Imagery layer with higher resolution Maxar Vivid basemaps in the Living Atlas.

Esri will use Maxar's Vivid basemaps to upgrade nearly half of the global landmass in Living Atlas from 1.2 m resolution to 60 cm resolution. This enhancement reflects a continued investment from the Esri Living Atlas team to bring the best quality, highest resolution imagery basemaps to ArcGIS Online users for creating more accurate maps and making better decisions.

The Living Atlas is a collection of geographic information from around the globe, including maps, apps and data layers. [www.maxar.com](http://www.maxar.com)

---

## NOAA inks pact with Planet to gain situational awareness of oil spills

Planet Labs PBC has announced a new contract with the National Oceanic and Atmospheric Administration (NOAA). The organization is leveraging Planet's PlanetScope and SkySat products to evaluate oil spills, track marine debris, detect vessels, and identify large marine mammals like whales. In 2004, Hurricane Ivan caused severe damage in the Gulf of Mexico, including the collapse and sinking of an oil platform. Crude oil from this platform continued to leak for over a decade, in what would become the longest running oil spill in United States history. NOAA began tracking the region with government-provided satellite data to generate reports on the situation. In 2018, NOAA reached out to Planet to explore how having a perspective of change on a near-daily basis around the platform could help inform their work.

Using PlanetScope imagery which provides near-daily imagery at 3 m resolution, NOAA set up an Area of Interest (AOI) around the leaking oil platform and received timely imagery of the region, supporting their evaluations of the quantity of oil leaking into the

surrounding environment. These updates were shared within their Marine Pollution Surveillance Report. Following this work, NOAA expanded their work with Planet, and today they observe a large region covering approximately 35,000 sq km in the Gulf of Mexico. [www.planet.com](http://www.planet.com)

---

## Near Space Labs launches Swiftly 3 stratospheric imaging robots

Near Space Labs has announced the launch of its Swiftly 3 fleet of advanced stratospheric imaging robots. The Swiftly 3 uses weather balloons and proprietary sensors and software to reach elevations nearly twice that of commercial flights, enabling the capture of incredibly high-resolution, high frequency images of landscapes, man-made structures, and changes occurring on the planet to help customers make critically strategic decisions.

The Swiftly 3 fleet of stratospheric imaging robots are low cost, manufactured in-house, and easily deployed in almost any location at a moments notice. <https://nearspace.com>

---

## Beyond Gravity launches "Launchpad"

The international space supplier Beyond Gravity is launching its start-up program "Launchpad" in October 2022. The incubator supports young start-ups and their promising ideas around space technology. In the process, teams are developed from an early stage to an initial investment opportunity. The application period runs until mid-August 2022.

From state-owned enterprise to start-up – Beyond Gravity (formerly RUAG Space) has set itself this maxim as its goal. With its own eight-week start-up program, it now offers young start-ups direct access to the international space community.

The three focal points of the incubator are space technology itself, the optimization of value chains, as well as the human factor in general, because we believe that people make the difference. The

first program will start in October 2022. [www.beyondgravity.com](http://www.beyondgravity.com)

---

## RS experts help scientists keep an eye on the Earth

Remote sensing experts from Rochester Institute of Technology are using innovative approaches to help scientists in government and the private sector monitor changes in the Earth's surface temperature. Scientists from RIT's Chester F. Carlson Center for Imaging Science recently helped successfully bring the new Landsat 9 satellite online and are partnering with a startup on a bold new initiative.

NASA and the U.S. Geological Survey's Landsat Program provides the longest continuous space-based record of Earth's land and RIT has supported the program dating back to the 1990s. The program launched its latest and most sophisticated satellite, Landsat 9, in September.

Since Landsat 9's launch, the RIT team has since been working to calibrate its thermal instrument and validate that it is producing consistent results. The calibration activities included an "underfly" event in November where Landsat 9 and its predecessor, Landsat 8, orbited the Earth in tandem to get a comparison of data collected by both. Aaron Gerace, research faculty and a member of RIT's Digital Imaging and Remote Sensing Laboratory, said that experiment leveraged data collected from unique temperature-sensing buoys developed by SUNY Oneonta Associate Professor Kiyoko [Yokota.rit.edu](http://Yokota.rit.edu)

---

## China launches new group of remote sensing satellites

China successfully launched a new group of remote sensing satellites from the Xichang Satellite Launch Center in southwest China's Sichuan Province on July 29.

The satellites were launched as the third group of the Yaogan-35 family at 9:28 p.m. (Beijing Time) by a Long March-2D carrier rocket and entered the planned orbit successfully. <https://english.news.cn>

## Baidu unveils next-gen autonomous vehicle

Baidu, Inc. has unveiled its next-generation fully autonomous vehicle (AV) Apollo RT6, an all-electric, production-ready model with a detachable steering wheel. It will be put into operation in China in 2023 on Apollo Go, Baidu's autonomous ride-hailing service.

Apollo RT6 integrates Baidu's most advanced L4 autonomous driving system, powered by automotive-grade dual computing units with a computing power of up to 1200 TOPS. The vehicle utilizes 38 sensors, including 8 LiDARs and 12 cameras, to obtain highly accurate, long-range detection on all sides. The safety and reliability of Apollo RT6 are backed by a massive trove of real-world data, a total test mileage of over 32 million kilometers (~20 million miles) driven by Baidu's AV to date. [baidu.com](https://baidu.com)

## Pony.ai and SANY to develop next-gen autonomous trucks

Pony.ai has announced a strategic joint venture with SANY Heavy Truck (SANY), China's heavy equipment manufacturer to create a world-leading autonomous truck brand. The two companies will deeply integrate Pony.ai's "virtual driver" with SANY's technical accumulation in the field of wire-controlled chassis and vehicle development to jointly develop high-end heavy trucks that are automotive-grade and have L4-class redundancies. <https://pony.ai>

## METIS & BUREAU VERITAS to advance augmented ship services

Bureau Veritas (BV), one of the world's leading ship classification societies, Laskaridis Shipping and METIS Cyberspace Technology who provides ship environmental and operational performance smart tools have agreed to embark on a pilot project to develop and apply a new BV SMART 3 Class notation covering the use of augmented data in ship operations.

Modern ships increasingly use smart systems designed to improve their operational efficiency. As part of its strategy to support maritime digitalization, BV has developed a framework of SMART notations for ships, which provide consistent and uniform standards for the 'smart' techniques used to monitor and improve fleet performance. <https://bureauveritas.com>

## Anari AI launched Thor X

A new Cloud-based technology "System-on-Cloud", developed by the Anari AI team, introduces an optimized and efficient system from various different hardware and software architectures combined with machine learning models to revolutionize the way AI compute systems are utilized. Anari AI is launching Thor X, the first "System-on-Cloud" specialized in semantic segmentation of 3D point cloud data structures. Primarily focused on providing custom hardware acceleration to industries such as geospatial, BIM, digital twin, and metaverse, Thor X is enabling 30x more efficient processing compared to the best GPUs on the market. <https://anari.ai>

## BAE Systems selected to advance autonomous technology

The Air Force Research Laboratory (AFRL) awarded BAE Systems a \$7.8 million contract to develop tightly integrated machine learning software as part of the Multi-Sensor Exploitation for Tactical Autonomy (META) program. This technology will enable advanced situational awareness and automatic target recognition (ATR).

Under the terms of the award, BAE Systems' FAST Labs™ research and development organization will provide Environmentally Adaptive Geospatial Learning and Exploitation, an innovative suite of machine learning and fusion algorithms. [baesystems.com](https://baesystems.com)

## Northrop Grumman and Airbus MOU

Northrop Grumman and Airbus have signed a Memorandum of Understanding to address the United Kingdom Ministry of Defence (MOD) military satellite communication system requirements as an integrated team. The team will work together to address future aspects of the SKYNET program ensuring that UK social value and industrial participation is maximised, and that the 'allied by design' approach is implemented to drive towards interoperability with key national allies. [www.northropgrumman.com](https://www.northropgrumman.com)

## Trimble introduces new scanning and imaging solution

Trimble has introduced the new Trimble X12 scanning system to the geospatial scanning portfolio. It integrates intuitive Trimble software for precise data capture and in-field registration with state-of-the-art 3D laser scanning and imaging hardware technology from Zoller+Fröhlich (Z+F), combining the expertise of two industry leaders into a single solution.

The Trimble X12 can be operated by using Trimble Perspective field software installed on a Trimble T10x tablet to enable registration and refinement of scans in the field, ensuring project accuracy and completion before leaving the jobsite. Users can also leverage Trimble's customized on-board software menu to configure and operate the scanner. Data is exported from the field and processed in the office with Trimble RealWorks™ software or third-party software. Final deliverables can be shared online with clients and stakeholders using Trimble Clarity, a browser-based data collaboration and visualization tool. [www.trimble.com](https://www.trimble.com)

## GeoSLAM technology deployed on large-scale urbanisation project

GeoSLAM's handheld LiDAR technology has been utilised to document informal settlements in one of India's largest cities, Bengaluru, as part of a large-scale urbanisation project. Geospatial mapping services company, Nakshatech,

surveyed the area and digitally mapped the informal settlements. Over the course of the three day project data was collected from more than 40 different areas of the settlements, automatically processing each dataset in its software.

Once compiled, orthophotos were created using the point cloud in GeoSLAM Draw, allowing the team to extract further information such as encroaching settlements. [www.geoslam.com](http://www.geoslam.com)

---

## Launching of Street View in India

Tech Mahindra and Google have announced a strategic partnership that licenses street-level imagery to Google toward the launch of their Street View feature in the country. The partnership will leverage output from Tech Mahindra's 'Gullyfy' project done in collaboration with eco-system partners, and is being carried out in accordance with the accuracy thresholds laid out in the geospatial guidelines. As a part of the partnership, Tech Mahindra will be responsible for GIS processes from data creation, resourcing, insights generation, and the actual collection of the street-level imagery. [www.techmahindra.com](http://www.techmahindra.com)

---

## Telit and Thales announce partnership

Telit and Thales have entered into an agreement under which Telit intends to acquire Thales' cellular IoT products. The intended transaction includes Thales' portfolio of cellular wireless communication modules, gateways, and data (modem) cards, ranging from 4G LTE, LPWAN to 5G. [www.telit.com](http://www.telit.com)

---

## Hexagon announces Leica BLK360 laser scanner

Hexagon AB has announced the introduction of the all-new, next-generation Leica BLK360, which dramatically advances reality capture by delivering two of the most sought-after necessities: speed and efficiency.

The new BLK360 creates stunning, photorealistic, accurate digital twins within just 20 seconds. Like its predecessor, it encourages new users to introduce reality capture to new industries and markets due to its speed, portability, and ease of use.

---

## Mapping the entire ocean floor

Terradepth and The Nippon Foundation-GEBCO Seabed 2030 project have announced a new partnership, which will utilize Terradepth's geospatial data portal known as Absolute Ocean. Seabed 2030 will use Absolute Ocean as a data visualization and exploration tool as part of the international effort to map the entire ocean floor.

Seabed 2030 is a collaborative project between The Nippon Foundation in Japan and the General Bathymetric Chart of the Oceans (GEBCO) with the mission of inspiring 100% mapping of the ocean floor and making it freely available to all by 2030. GEBCO is a joint program of the International Hydrographic Organization (IHO) and the Intergovernmental Oceanographic Commission of UNESCO (IOC-UNESCO). Seabed 2030 comprises five Data Centers – four Regional Centers and one Global Center – which are responsible for coordinating and assembling mapping data.

In addition to producing and delivering global GEBCO products, the Seabed 2030 Global Center is also a Trusted Node for receipt of citizen-sourced data in support of IHO's Crowdsourced Bathymetry (CSB) initiative which encourages government, academic and privately owned vessels, including superyachts and fishing boats, to participate in increasing our knowledge of the ocean by sharing depth measurements from navigation instruments. <https://seabed2030.org>

---

## First cloud-connected cockpit system

Cyient has announced a partnership with Honeywell to manufacture the aviation industry's first cloud-connected cockpit system – The Honeywell Anthem. Cyient has inked a multi-year deal with Honeywell for this project. With design validation for electronics, Cyient will provide turnkey manufacture and testing of multiple LRUs that comprise the Honeywell Anthem avionics suite. With the help of Cyient's supply chain management technologies and Industry 4.0 linked plants, Honeywell will obtain predictable delivery schedules and continuous quality improvement over the program's life. [www.cyient.com](http://www.cyient.com)

---

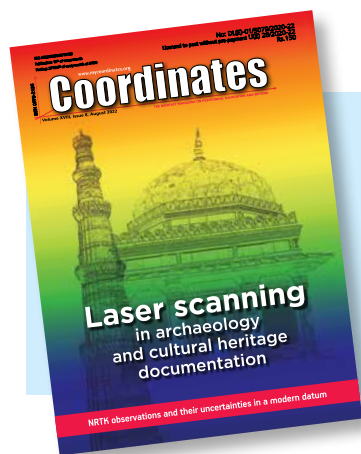
## Drone Package

The E300 drone package includes the E300 real-time kinematic (RTK) drone, flight-control software and an optional camera. The drone is embedded with a high-precision K8 GNSS module that supports GPS L1/L2/L5, BeiDou B1/B2/B3/B1C/B2a, GLONASS L1/L2, Galileo E1/E5-a/E5-b/AltBOC/E6 and QZSS L1/L2/L5. With its intelligent recognition algorithms, the E300 can capture high-resolution images consistently even in complex environments. [comnav.com](http://comnav.com)

---

## New Timing Antenna by Tallysman

Tallysman® Wireless recently introduced the housed TW3885T dual-band (L1/L5) Accutenna® technology timing antenna. The antenna supports GPS/QZSS L1/L5, Galileo E1/E5a/b, BeiDou B1/B2/B2a, GLONASS G1/G3 and in



“The monthly magazine on Positioning, Navigation and Beyond”

Download your copy of  
Coordinates at  
[www.mycoordinates.org](http://www.mycoordinates.org)

the region of operation, satellite-based augmentation systems (SBAS): WAAS (North America), EGNOS (Europe), MSAS (Japan), or GAGAN (India).

The antenna is housed in a through-hole mount, weatherproof (IP69K) enclosure. L-bracket (PN 23-0040-0) or pipe (23-0065-0) mounts are available for permanent installations.

---

### Hi-Target launches vRTK receiver with GNSS, IMU and cameras

Hi-Target has launched a real-time-kinematic (RTK) GNSS receiver that has an eye for visual positioning. The pocket-sized vRTK GNSS RTK System is equipped with professional dual cameras to enable non-contact image surveying. It also has an advanced inertial measurement unit (IMU).

vRTK is suitable for non-contact measurements in a variety of hazardous and complex environments. High-quality sensors ensure the stability of the receiver's accuracy in working status. By combining imagery with high-precision positioning equipment, users benefit from the convenience of visual positioning technology, which allows them to obtain the location of the target with a touch of a finger from a distance. <https://en.hi-target.com.cn>

---

### GMV wins European NAVGUARD contract for Galileo PRS

GMV has been awarded the NAVGUARD project by the European Commission.

NAVGUARD (Advanced Galileo PRS Resilience for EU Defence) will develop ground and space systems to detect illegal activities on GNSS frequencies and geolocate their sources. It also will build an information-management subsystem together with a user interface to provide a situational awareness picture.

The Galileo Public Regulated Service (PRS) is an encrypted navigation service for governmental authorized users and sensitive applications that require high continuity.

According to the EU Agency for the Space Programme (EUSPA), the PRS signal will ensure better continuity of service to authorized users when access to other navigation services may be degraded (resilience). In cases of malicious interference, PRS increases the likelihood of the continuous availability of the signal-in-space (robustness).

NAVGUARD is among various European Defence Fund (EDF) projects designed to sharpen the competitiveness of the European Union defense industry and strengthen the EU's strategic autonomy. Besides navigation, the projects contracted to GMV will focus on developing missile defense system capabilities, systems for dismounted soldiers, avionics, command and control and cyber defense. [www.gmv.com](http://www.gmv.com)

---

### Locating Shackleton's historic endurance vessel

Having been lost for more than 100 years beneath more than 3,000 metres of sea ice in the Antarctic's Weddell Sea, the almost fully intact wreck of Ernest Shackleton's Endurance has been found, supported with underwater navigation and positioning technology from Sonardyne.

The pioneering search, launched in February this year, saw the Endurance22 team deploy Saab Seaeye Sabertooth hybrid autonomous underwater vehicles (AUVs) from the ice-breaking polar supply and research ship SA Agulhas II.

During their hunt of the seabed, close to where the 1914–1917 expedition came to its end, these underwater robots used Sonardyne's SPRINT-Nav hybrid acoustic-inertial navigation system (INS) technology to navigate their search routes. They also used its AvTrak 6 tracking and telemetry transceiver, to send commands and position updates from a Ranger 2 Ultra-Short BaseLine (USBL) system, onboard the SA Agulhas II.

For ease of deployment, the Ranger 2 was configured with a Gyro USBL transceiver. This comes with an inbuilt

attitude, heading and reference sensor (AHRS) and is pre-calibrated, making it easy to deploy on vessels of opportunity. A second Ranger 2 Gyro USBL system was also on hand, ready to be deployed from the surface of the ice if the SA Agulhas was unable to get through the Weddell Sea's sea ice. Both were LMF systems, enabling tracking at ranges beyond 7,000m, to meet the Endurance22 team's potential under-ice tracking requirements.

---

### High-accuracy mapping solution for GIS field applications by Trimble

Trimble recently announced a new high-performance data collector for its Mapping and GIS portfolio—the Trimble® TDC650 handheld. Built for GIS data collection, inspection and asset management activities, the TDC650 provides users a rugged solution with scalable high-accuracy GNSS positioning for professional field workflows. [www.trimble.com](http://www.trimble.com)

---

### Dual-band GNSS timing receiver for the OCP-TAP

Protempis (formerly Trimble's Time and Frequency Division) has announced that the company is providing its industry-leading dual-band timing receiver Res720 embedded module for Open Compute Project Time Appliance Project (OCP-TAP) open-sourced time card reference design. The module is an ideal solution for data center, 5G Open RAN / XHaul, smart grid, industrial automation, and SATCOM networks. It provides unparalleled performance with five nanosecond timing accuracy, dual-band GNSS support, and anti-jamming/anti-spoofing capabilities.

In 2020, OCP-TAP started working on highly precise and hyper scalable time synchronization services in its data center market, using a GNSS clock source[es] and Precision Time Protocol (PTP) technologies. OCP-TAP technology adds scalability and improves the accuracy of timekeeping within the infrastructure industry. In 2021, OCP-TAP integrated its technology into the Time Card and

# SUBSCRIPTION FORM

YES! I want my **Coordinates**

I would like to subscribe for (tick one)

1 year     2 years     3 years

12 issues

24 issues

36 issues

Rs.1800/US\$140

Rs.3400/US\$200

Rs.4900/US\$300

\*

**SUPER  
saver**

First name .....

Last name .....

Designation .....

Organization .....

Address .....

City ..... Pincode .....

State ..... Country .....

Phone .....

Fax .....

Email .....

I enclose cheque no. ....

drawn on .....

date ..... towards subscription

charges for Coordinates magazine

in favour of 'Coordinates Media Pvt. Ltd.'

Sign ..... Date .....

Mail this form with payment to:

Coordinates

A 002, Mansara Apartments

C 9, Vasundhara Enclave

Delhi 110 096, India.

If you'd like an invoice before sending your payment, you may either send us this completed subscription form or send us a request for an invoice at [iwant@mycoordinates.org](mailto:iwant@mycoordinates.org)

\* Postage and handling charges extra.

## MARK YOUR CALENDAR

### September 2022

International Symposium of Commission

4: Positioning and Applications

5 to 8 September 2022

[www.iag-commission4-symposium2022.net](http://www.iag-commission4-symposium2022.net)

15th Conference on Spatial

Information Theory (COSIT)

5-9 Sep 2022

Kobe, Japan

[cosit2022.iniad.org](http://cosit2022.iniad.org)

Commercial UAV Expo Americas

6-8 September 2022

Las Vegas, USA

[www.expouav.com](http://www.expouav.com)

17th Symposium on Location

Based Services (LBS2022)

12-14 Sep 2022

Munich, Germany

[lbsconference.org](http://lbsconference.org)

18th International Conference on

Geoinformation and Cartography

14-16 Sep 2022

Zagreb, Croatia

[www.kartografija.hr](http://www.kartografija.hr)

EuroCarto 2022

19-21 Sep

Vienna, Austria

[www.eurocarto2022.org](http://www.eurocarto2022.org)

ION GNSS+ 2022

19-23 September

Denver, CO, USA

[www.ion.org/gnss/index.cfm](http://www.ion.org/gnss/index.cfm)

### October 2022

2<sup>nd</sup> United Nations World Geospatial

Information Congress (UNWGIC)

10-14 October 2022

Hyderabad, India

<https://ggim.un.org/2unwgic>

The 7<sup>th</sup> Geospatial Conference

The 6<sup>th</sup> SMPR and 4<sup>th</sup> GIREsearch

15-18 October 2022

Tehran, Iran

<https://geospatialconf2022.ut.ac.ir>

Intergeo Hybrid

18-20 October 2022

Essen, Germany

[www.intergeo.de](http://www.intergeo.de)

### November 2022

Trimble Dimensions+

7-9 November 2022

Las Vegas, USA

<https://dimensions.trimble.com>

introduced it as an open-source solution to build time servers. [protempis.com](http://protempis.com)

## Quectel launches single-band GNSS module

Quectel Wireless Solutions released its LC76G module, a single-band compact GNSS module featuring fast and accurate location performance as well as ultra-low power consumption. The LC76G has already entered mass production with sufficient supply to meet the needs of the global positioning market. [www.quectel.com](http://www.quectel.com)

## GEODNET base-station by HYFIX.AI

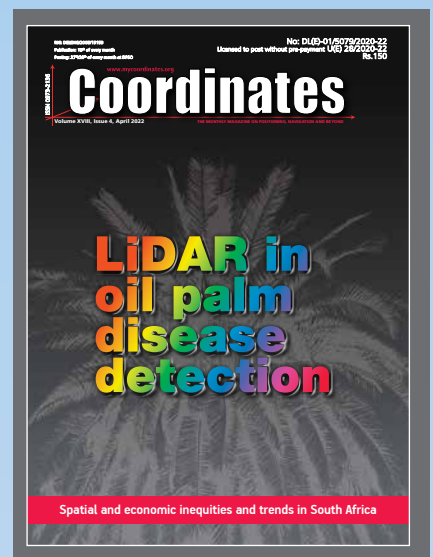
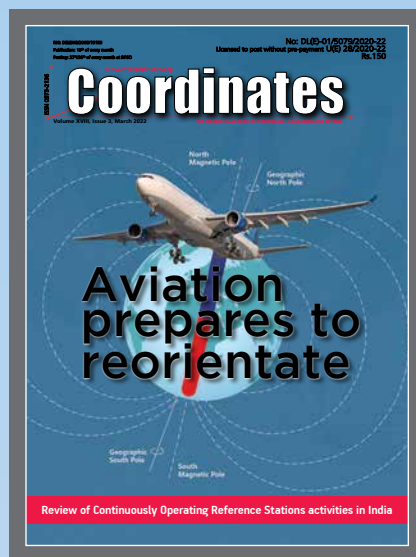
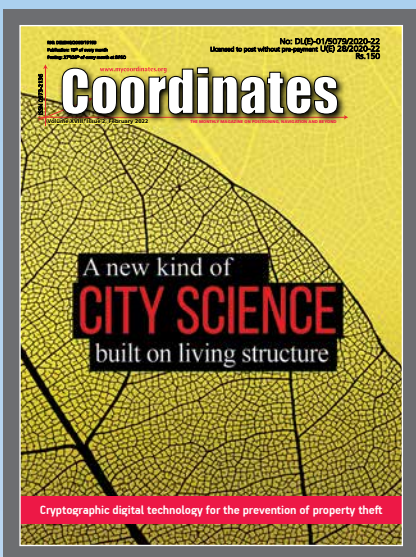
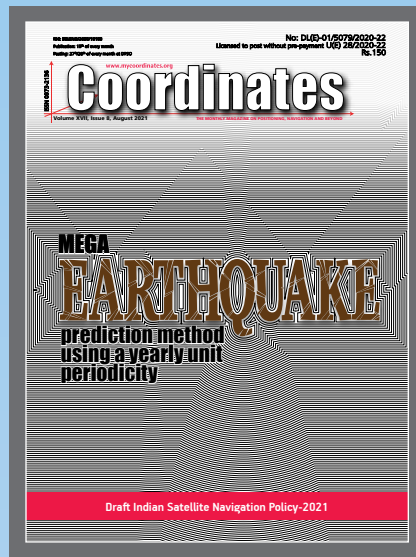
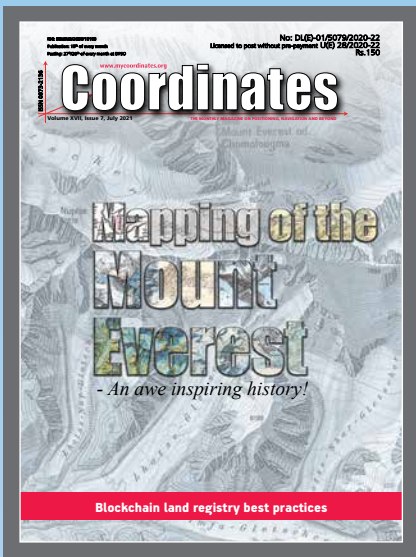
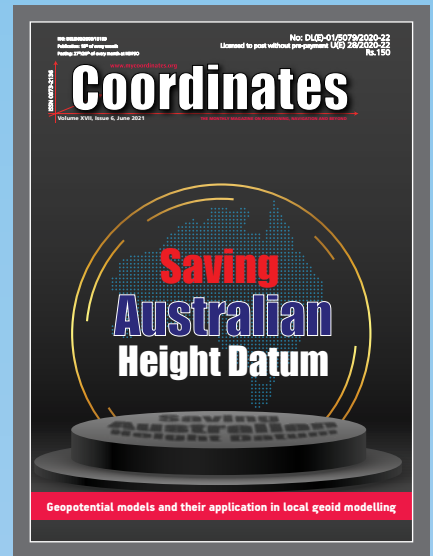
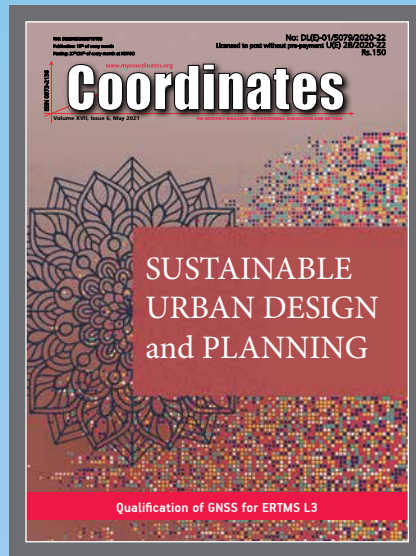
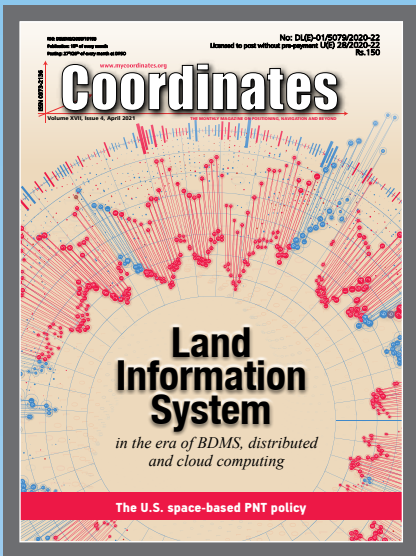
HYFIX.AI announces the availability of a GEODNET base-station using the LC29H module from Quectel Wireless Solutions.

The Mobile Centimeter (MobileCM) base-station is a dual-band GNSS base-station for Real-Time Kinematic (RTK) precise-positioning applications in Autonomy, Agriculture, Construction/Survey, Drones and Geo-Science applications. [www.quectel.com](http://www.quectel.com)

## Korea's first convenience store drone delivery station

PABLO AIR, in cooperation with South Korea's 7-Eleven branch, has opened the first convenience store drone delivery station in Korea for the commercialization of drone delivery. It primarily consists of a control tower and the drone's vertical take-off and landing aerodrome (Helipad), which allows one-stop processing, from the taking of delivery orders to the completion of the delivery flight. The drone delivery service is a beyond visual line of sight (BVLOS) flight in which the drone is controlled with a wGCS (Web-based Ground Control System) paired with a smart mobility integrated control system (PAMNet, PABLO AIR Mobility Network) for safe and agile operation of the aircraft.

In June, the Korean government promised to ease regulations and establish a legal basis for the drone delivery industry as part of its new industry regulation improvement plan. [pabloair.com](http://pabloair.com)



“The monthly magazine on Positioning, Navigation and Beyond”  
Download your copy of Coordinates at [www.mycoordinates.org](http://www.mycoordinates.org)



## Cost-effective and reliable End-of-Line testing for any GNSS receiver

LabSat 3 is a lightweight, portable and affordable GNSS simulator - an ideal test partner for Production Line and End-of-Line (EOL) testing.



### Multi-Constellation

Record & Replay up to 3 frequency bands and 4 constellations



### Developer API

Automate tests with centralised control available via ethernet connection



### Bespoke Scenarios

Use SatGen software to create bespoke simulation scenarios at any time and location



### Cost Effective

Options to suit any budget - starting from \$5,495

RECORD / REPLAY / SIMULATE

[labsat.co.uk/eol](http://labsat.co.uk/eol)